EUROPEAN ORGANIZATION FOR NUCLEAR RESEARCH

CERN – AB DEPARTEMENT

CERN-AB-2005-010

Simulation of Transient Effects of Beam-Transverse Feedback Interaction with Application to the Extraction of the CNGS Beam from the SPS

W. Hofle, E. Vogel

Abstract

For existing and future high energy proton accelerators, transverse feedback systems play an essential role in supplying the physics experiments with high intensity beams at low emittances. We developed a simulation model to study the interaction between beam and transverse feedback system in detail, bunch-by-bunch and turn-by-turn, considering the technical implementation at the SPS [1]. A numerical model is used as the non linear behaviour (saturation) and limited bandwidth of the feedback system, as well as the transient nature at injection and extraction, complicates the analysis.

The model is applied to the practical case of the CNGS beam [2] in the SPS accelerator. This beam will be ejected from the SPS in two batches causing residual oscillations by kicker ripples on the second batch. This second batch continues to circulate for 50 ms (about 2170 turns) after the first batch has been extracted and oscillations are planned to be damped by the feedback system.

Geneva, Switzerland

January 2005

Contents

1 Introduction

For existing and future high energy proton accelerators, transverse feedback systems play an essential role in supplying the physics experiments with high intensity beams at low emittances. They stabilize beams whose parameters are otherwise far away from stable regions. Hence, they have a significant influence on beam dynamics.

The interaction between the beam and a feedback system depends strongly on the real technical implementation and limitations of the latter. Limited available correction kick strengths and limited bandwidths are typical features. The resulting behaviour can be examined, by performing numerical simulations.

Experimental verification of the simulation model is essential. For future tests of our initial simulation model we have chosen a particular beam condition in the SPS for which the beam is relatively stable – this is with CNGS type beams at extraction energy. It is later planned to extend the model to include beam instabilities for the examination of other operational conditions and other accelerators (e.g. the LHC).

The CERN neutrinos to Gran Sasso (CNGS) experiment [2] requires two SPS batches of 400 GeV proton beams to be shot 50 ms in succession onto a graphite target creating pions and kaons. These particles decay into muons and neutrinos, resulting finally in a neutrino beam propagating 732 km through the earth towards the neutrino detector located in Gran Sasso (Italy).

Tight constraints have to be met concerning the extraction kick angle to properly hit the target 590 m downstream of the extraction from the SPS. In addition, the rising and falling edges of the extraction kicker field have to be shorter than the gaps between the two batches, in order to extract the first batch without influencing the one which is still circulating. This condition is not perfectly fulfilled. Bunches of the second batch will also receive kicks during the first extraction, leading to transverse beam oscillations. Because of the large decoherence time of about 10 000 turns [3], the oscillations will persist. At the extraction of the second batch, about 2170 turns later, the bunches still oscillating will not hit the CNGS target properly. Almost all bunches of the second batch will have the wrong transverse position on the target.

The transverse coupled bunch feedback system in the SPS is designed to damp injection oscillations and stabilize coupled bunch oscillations. It is not designed to provide rapid damping of large oscillation amplitudes at top energy, such as induced by the extraction kicker ripple and finite kicker rise time. When damping these oscillations with a high gain, the feedback amplifiers can become saturated. In this non-linear regime higher coupled bunch modes may no longer be damped.

We use Simulink [4], a Matlab extension for modelling, simulating and analyzing dynamic systems. Its graphical user interface allows a representation of the complete system by 'drawing' the corresponding signal flow diagram. This is very efficient in saving development and code implementation time. A large library of standard building blocks is available, e.g. several kinds of filters. Signal sources are available for exciting the systems, just as graphical representations for the output signals, like scopes.

Simulink is able to translate the graphical block diagrams into C and compile the result. Using this feature, we observed an increase of the simulation speed by a factor of 10. Whether an identical code runs faster by a direct implementation in C will have to be checked in the future. In such a case Simulink may serve as prototype platform.

2 Main components

Figure 2.1 shows the main components of the CNGS extraction simulation. The extraction kicker deflects the beam only horizontally. Hence, we can restrict our examinations to one plane. In this chapter, we will give an overview, before going into the details in the following chapters.

The first central part of the simulation model describes the horizontal oscillations of the CNGS type beams in the SPS without coupling impedance. Emittance blow up by decoherence is taken into consideration using algebraic expressions, bunch-by-bunch and turn-by-turn [5]. The model offers inputs for injecting and extracting bunches together with bunch parameters such as injection offsets, normalized bunch sizes, kick angles caused by extraction kickers and the electric field value of the feedback kicker. Further input values are the tune and the total particle energy. Output values are beam position signals measured at two beam monitors. For diagnostic purposes the normalized bunch size, a marker showing whether a bunch position is occupied or not and the betatron oscillation amplitude are supplied.

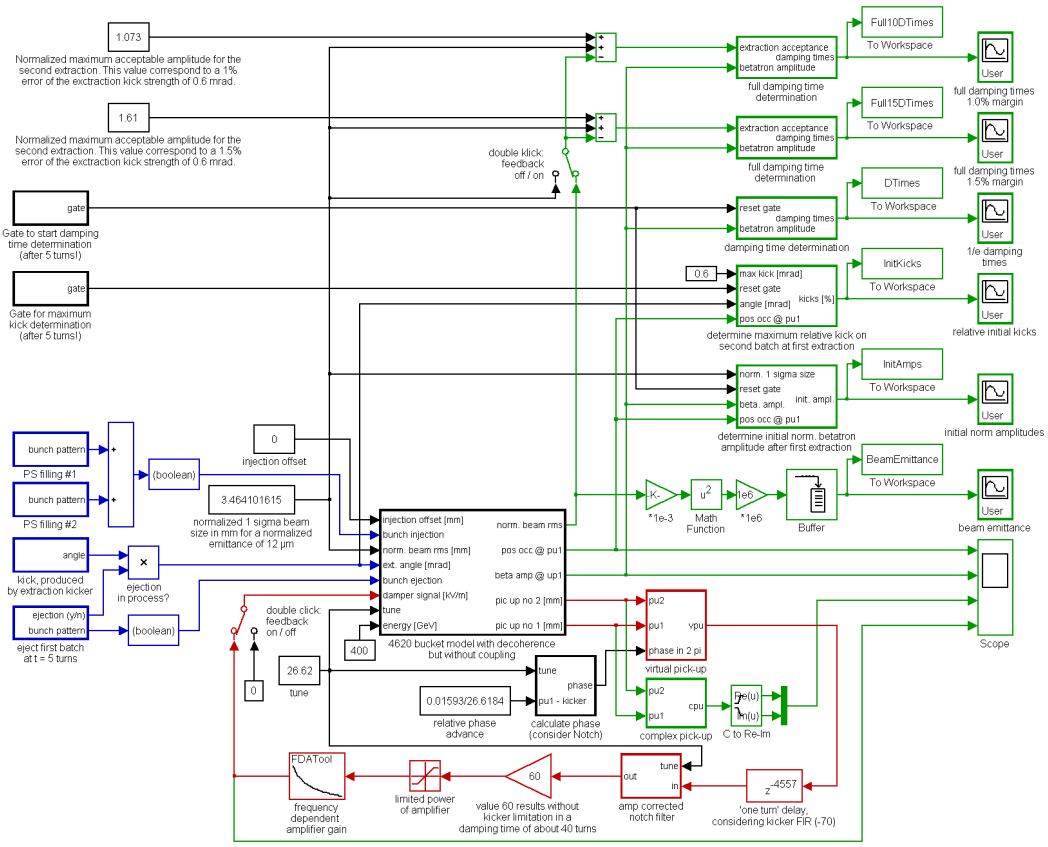

Figure 2.1: The main components of the simulation: 4620 bucket model for CNGS type beam in the SPS (center), the feedback loop (red), time pattern and kick values for injection and extraction (blue), diagnostics (green) and some initial values.

The second central part is the transverse feedback, with the essential components of the

actual system. The first step in signal processing is the combination of the signals of the two beam position monitors into a single signal to ensure the necessary feedback phase. A one turn delay is implemented by a first-in, first-out (FIFO) buffer, guaranteeing that a measured transverse position of a bunch leads to a signal applied to the same bunch. A periodic notch filter, with zeros at multiples of the revolution frequency, supresses the signal caused by the sampling of closed orbit distortions. The behaviour of the final stage amplifier, together with the connected kicker, is described by a limiter and a finite impulse response (FIR) filter. These elements model the limited power and the gain frequency characteristics with lower gain for higher frequencies. The overall loop gain is adjusted by changing a gain value in front of the limiter. The feedback in the simulation may be switched on and off.

At the start of a simulation, the beam model describes an empty accelerator. Bunches with specific bunch sizes must first be 'injected', attention being paid to the timing to obtain the correct filling pattern. The 'extraction' acts in the same way. Within the turn that extraction of the first batch takes place, kicks are applied to the bunches of the second batch. All these time-dependent patterns for injection and extraction are the main input values for the beam model.

Beam and feedback parameters, like occupied bunch positions, betatron oscillation amplitudes at one pick-up, the 'complex' betatron amplitudes and the voltage at the kickers are shown in the time domain on a virtual oscilloscope. The betatron oscillation amplitudes and the normalized rms bunch sizes are analyzed to check whether the CNGS target constraints are fulfilled. The damping times and the times until CNGS constraints are fulfilled ('full damping times') are determined. Furthermore, the normalized emittance of each bunch is calculated.

3 The 4620 bucket model

The block '4620 bucket model ...' in Figure 2.1 contains the beam dynamics. It takes into account population patterns and the values of the optics functions at the points of the injection, extraction, beam position monitors and the feedback kickers. The beam blow up is considered via an algebraic computation [5, 6]. Figure 3.1 shows the structure of the model, the details of which are described in the following sections.

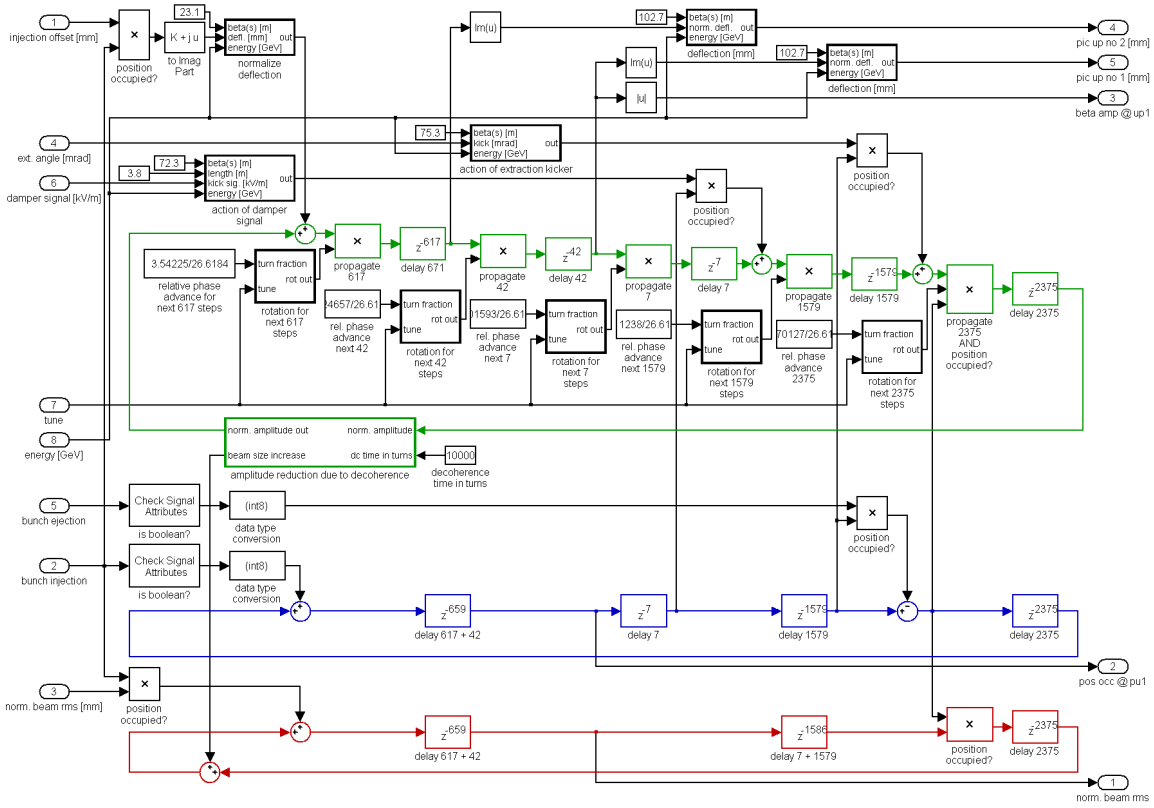

Figure 3.1: The 4620 bucket model describing the beam dynamics with three loops: Betatron amplitude loop (green), bucket population loop (blue) and the loop containing the rms bunch sizes (red).

3.1 Rigid bunch tracking

In the SPS, every RF bucket is filled for CNGS type beams, except for two gaps. The RF system operates with 200 MHz, resulting in a bunch spacing of 5 ns. Hence, we use for the simulation discrete time steps of one revolution divided by the harmonic number, i.e. $1/4620$. For simplicity, we deal only with two physical parameters per bunch, the horizontal bunch centre[1] (rigid bunch) and the horizontal r.m.s. beam size.

[1] We use 'bunch centre' as a synonym for the centre of gravity of a bunch.

We describe the betatron oscillations of the bunch centres in an energy normalized way. Such a description is more flexible in case the particle energy is changed. This also simplifies the calculation of the beam blow up, as shown later.

The solution of the equation of motion of a particle in a circular accelerator is in the transverse case [7]

$$x\left(l\right) = A\sqrt{\beta_{\mathrm{x}}\left(l\right)}\cos\left(\Psi\left(l\right)+\phi\right) \qquad \text{with} \quad \Psi\left(l\right) = \int_0^l \frac{d\,\xi}{\beta_{\mathrm{x}}\left(\xi\right)}. \tag{3.1}$$

The transverse position x depends on the longitudinal coordinate along the accelerator l, the betatron amplitude A, the betatron amplitude function $\beta_{\mathrm{x}}\left(l\right)$ and the betatron phase $\Psi\left(l\right)$. ϕ is a constant phase factor depending on the initial boundary conditions. A particle, with oscillation amplitude equal to $1\sigma_{\mathrm{x}}$ of the particle distribution, has an oscillation amplitude A_{rms} equal to the square root of the beam rms emittance ϵ

$$A_{\mathrm{rms}} = \sigma_{\mathrm{x}} = \sqrt{\epsilon}.$$

The value of the 'normalized emittance'

$$\epsilon_{\mathrm{n}} = \beta\,\gamma\,\epsilon \qquad \text{with} \quad \beta = \sqrt{1-\left(\frac{E_0}{E}\right)^2} \quad \text{and} \quad \gamma = \frac{E}{E_0}$$

remains constant during acceleration in the ideal case. Perturbing effects lead to an increase. E is the particle total energy and $E_0 = m_{\mathrm{p}}\,c^2$ the proton rest energy.

We obtain an energy independent description of the betatron oscillation by introducing a 'normalized oscillation amplitude' A_{n} as follows[2]

$$A_{\mathrm{n}} = \sqrt{\beta\,\gamma}\,A$$

and verify that this is consistent with the definition of the normalized emittance:

$$A_{\mathrm{rms}} = \frac{A_{\mathrm{n,rms}}}{\sqrt{\beta\,\gamma}} = \frac{\sqrt{\epsilon_{\mathrm{n}}}}{\sqrt{\beta\,\gamma}} = \sqrt{\epsilon}.$$

We rearrange (3.1) and describe the betatron oscillation in a normalized way:

$$x_{\mathrm{n}}\left(l\right) \equiv x\left(l\right)\sqrt{\frac{\beta\,\gamma}{\beta_{\mathrm{x}}\left(l\right)}} = A_{\mathrm{n}}\cos\left(\Psi\left(l\right)+\phi\right). \tag{3.2}$$

The betatron phase $\Psi\left(l\right)$ is linked to the β-function, as (3.1) indicates. Hence, the number of betatron oscillations within one revolution, that is the tune Q, is given by

$$Q = \frac{\Psi\left(2\pi R\right)}{2\pi} = \frac{1}{2\pi}\int_0^{2\pi R} \frac{d\,\xi}{\beta_{\mathrm{x}}\left(\xi\right)}.$$

Here, $2\pi R$ is the length of the particle orbit.

In practice the magnetic field of quadrupole magnets in an accelerator is varied in order to adjust the tune. These variations lead to local changes of the β-function at the magnet positions. A transverse feedback system 'interacts' with the beam only at a few points in the accelerator.

[2] note $[A] = [A_{\mathrm{n}}] = \sqrt{\mathrm{m}}$

Main interaction points are at the beam position monitors and the feedback kickers. For the betatron phase at these points, it is of secondary importance as to whether variations of the β-function are localized at the magnet positions or equally spread over the accelerator, because of the integral dependence (3.1). Hence, we determine only once the betatron phase $\Psi_{\mathrm{mad}}(l)$ with an optics program like MAD. For this determination, the tune value Q_{mad} is ideally equal to the value Q, used for the simulations. In case Q, used in the simulation, differs from Q_{mad}, we assume the optics changes are equally spread over the accelerator and recalculate the betatron phase with

$$\Psi(l) \approx \frac{Q}{Q_{\mathrm{mad}}}\,\Psi_{\mathrm{mad}}(l)\,. \tag{3.3}$$

By this approximation, the maximum error in the phase advance between two positions l_2 and l_1 is

$$\frac{\Delta\left(\Psi(l_2)-\Psi(l_1)\right)}{\Psi(l_2)-\Psi(l_1)} \leq \frac{|Q-Q_{\mathrm{mad}}|\cdot|\Psi_{\mathrm{mad}}(l_2)-\Psi_{\mathrm{mad}}(l_1)|}{Q_{\mathrm{mad}}}.$$

The phase advance between beam position monitors and feedback kicker is most important. Its value has an effect on the simulation on each turn. At the SPS, (in the horizontal plane) the phase advance between the beam position monitors and the feedback kicker is smaller than $\frac{\pi}{4}$. In the case where Q differs from $Q_{\mathrm{mad}} = 26.6184$ by 0.1, the error in phase is smaller than $0.3°$. This is negligible.

The phase advance between the extraction (injection) kickers and the elements of the feedback system is only relevant for the turn where the extraction (injection) takes place. Assuming again a tune difference of 0.1 results in an upper limit for the error of $12.7°$. Such errors may become important in case of feedback damping times smaller than 20 turns. This is not the case at the extraction of CNGS beam.

The oscillations can efficiently be described via angular pointers and complex numbers respectively. We define that the normalized horizontal beam position x_{n} at a position l is given by the imaginary part of the normalized complex betatron amplitude $\mathbf{A}_{\mathrm{n}}$:

$$x_{\mathrm{n}}(l) = \mathrm{Im}\,\mathbf{A}_{\mathrm{n}}(l) \qquad \text{with} \quad \mathbf{A}_{\mathrm{n}}(l) = \underbrace{A_{\mathrm{n}}\exp\left(i\left(\phi+\frac{\pi}{2}\right)\right)}_{=\mathbf{A}_{\mathrm{n}}(0)}\exp\left(i\,\frac{Q}{Q_{\mathrm{mad}}}\,\Psi_{\mathrm{mad}}(l)\right) \tag{3.4}$$

From the complex betatron amplitude at the position l_1, we calculate the value at the downstream position l_2 with

$$\mathbf{A}_{\mathrm{n}}(l_2) = \mathbf{A}_{\mathrm{n}}(l_1)\exp\left(2\pi\,i\,Q\,\frac{\Psi_{\mathrm{mad}}(l_2)-\Psi_{\mathrm{mad}}(l_1)}{2\pi\,Q_{\mathrm{mad}}}\right). \tag{3.5}$$

This relation is used for tracking the complex oscillation amplitudes in the simulation from one interaction point to the next.

The division of the time in steps of the bunch spacing leads to a granularity for the propagation time from one point to the next. This does not affect the betatron phase advance between the points. Signals propagating through the feedback are anyway delayed by about one revolution. An exact modeling of the time would only lead to minor changes in the time delay values. Hence, the time granularity has no further relevance for the results of the simulation.

Table 3.1 contains the elements used in the simulation and their positions. For simplicity we reduced the actions of longer structures to actions at single points. For example, instead of treating all extraction kickers, we replace them by one kicker acting equally.

Now, we have all the ingredients necessary for simulating betatron oscillations of a multi bunch beam circulating in the SPS. The implementation in Simulink is very intuitive. We build

Table 3.1: Positions and horizontal betatron phase (for $Q_{\mathrm{mad}} = 26.6184$) of the elements, relevant for the simulation, their positions, relative distances in simulation steps (of 5 ns each) and phase advance between them. The values of the horizontal β-function are also given.

Element (optics name)	l in m	$\beta_{\mathrm{x}}(l)$ in m	$\Psi_{\mathrm{mad}}(l)$ in 2π	$\frac{4620}{6911.6\ \mathrm{m}}\ l$	steps to next element used ($\times 5$ ns)	$\Delta\Psi_{\mathrm{mad}}$ to next element in 2π
first injection kicker (MKPA11931)	613.38	23.12	2.37237	410	617	3.54225
last injection kicker (MKPB11952)	620.63	36.27	2.41260	not used		
beam position monitor no 2 (BPH21209)	1535.66	102.69	5.91462	1027	42	0.24657
beam position monitor no 1 (BPH21409)	1599.65	102.67	6.16119	1069	7	0.01593
horiz. damper kicker no 1 (BDH21437)	1609.12	77.18	6.17712	1076	1579	9.11238
horiz. damper kicker no 2 (BDH21451)	1611.70	67.44	6.18281	not used		
first extraction kicker (MKE41631)	3972.34	95.56	15.2895	2655	2375	13.70127
last extraction kicker (MKE41654)	3981.60	61.09	15.3089	not used		

up a loop containing discrete delay blocks, where the sum of all delays is the number of bucket positions, i.e. 4620. Each delay block acts as a first-in, first-out (FIFO) buffer. The buffer depth is the specified delay value. In this way 4620 complex betatron amplitude values are circulating in the loop. The delay blocks are arranged in such a way that a certain value needs the number of simulation steps, given in Table 3.1, to move from element to element. In addition to the transport, the complex betatron amplitude values have to be updated in accordance with (3.5).

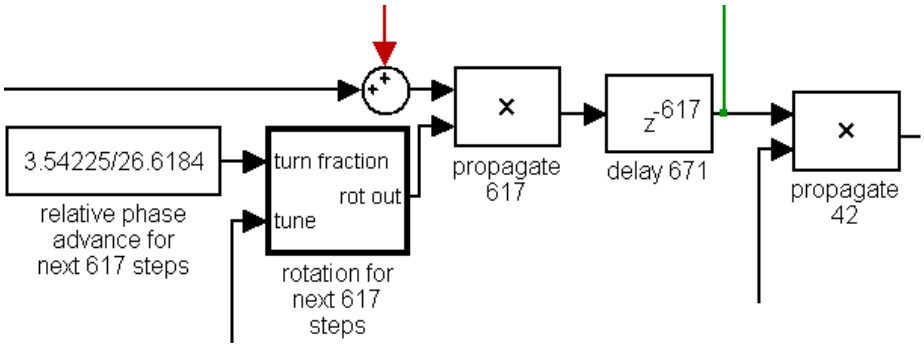

Figure 3.2: Tracking between injection (red) and second beam position monitor (green).

Figure 3.2 shows the part of the loop between injection and the beam position monitor no 2. Firstly, the exponential function of (3.5) is calculated in the 'rotation for ...' block from the relative MAD phase advance between both elements and the actual tune. The result is multiplied by the complex betatron amplitude to obtain the input value for the next element. The result is then 'stored' for 617 simulation steps by the delay block before it emerges at the beam position monitor.

The remaining parts of the loop, shown in Figure 3.1, work in the same way, except for the 'amplitude reduction ...' block. We will discuss this block later. For infinite decoherence times it has no influence on the circulating complex betatron amplitude values.

3.2 Bucket population and beam injection

It is not possible to decide from the value of the complex betatron amplitude whether a bucket is populated or not. Zero values may indicate either empty buckets or bunches without oscillations. Hence, a second loop with circulating binary values has to indicate whether a bucket position is populated '1' or not '0'. We call this loop the 'population loop'. Furthermore, it would be useful to study effects on the beam size with our simulation. Therefore a third loop contains the normalized r.m.s bunch sizes. For these loops, see Figures 3.1 and 3.3.

At the start of a simulation, all values in the loops are zero. This is equivalent to an empty accelerator, in which we first have to inject. For injecting a bunch the value '1' is provided to the 'bunch injection' input of the 4620 bucket model. It is added to the actual value at the injection point of the population loop and marks the bucket as populated (see Figure 3.3). At the same time, the value at the 'injection offset' input is converted and inserted (added) into the complex betatron amplitude loop. This is also the case for the normalized r.m.s. beam size. The code does not check whether a bunch is injected into a bucket already populated. Care has to be taken to ensure that this is not the case!

The code presented considers only injection offsets and not injection angles. This is sufficient for code debugging purposes as we will not study injection processes. An injection with offset x_{inj} results in a betatron oscillation. According to (3.2) and (3.4) this oscillation is described by a complex betatron amplitude at the injection point $\mathbf{A}_{\mathrm{n}}\left(l_{\mathrm{inj}}\right)$ of which the imaginary

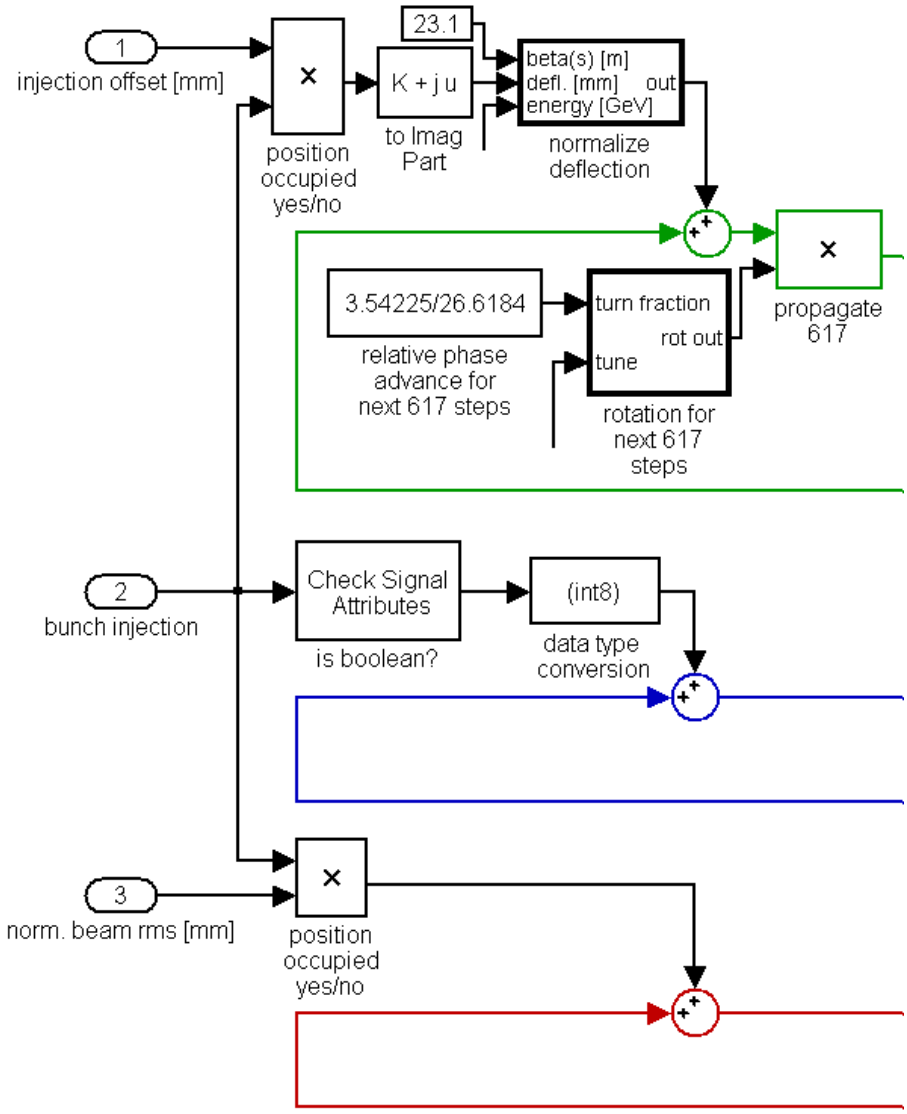

Figure 3.3: Scheme of Simulink code, relevant for injections. All parts of the code irrelevant for the injection process are omitted. An 'injection' into the occupation loop (blue) results also in an injection into the complex amplitude loop (green) and the r.m.s. bunch size loop (red).

part contains the normalized offset value

$$\operatorname{Im} \mathbf{A}_{\mathrm{n}}\left(l_{\mathrm{inj}}\right)=\sqrt{\frac{\beta\,\gamma}{\beta_{\mathrm{x}}\left(l\right)}}\,x_{\mathrm{inj}} \qquad \text{and} \qquad \operatorname{Re} \mathbf{A}_{\mathrm{n}}\left(l_{\mathrm{inj}}\right)=0.$$

3.3 Measured transverse beam position

From the values of the complex betatron amplitude at a beam position monitor $\mathbf{A}_{\mathrm{n}}\left(l_{\mathrm{pu}}\right)$ we calculate the beam position value x_{pu} considering (3.2) and (3.4)

$$x_{\mathrm{pu}}=\sqrt{\frac{\beta_{\mathrm{x}}\left(l_{\mathrm{pu}}\right)}{\beta\,\gamma}}\,\operatorname{Im} \mathbf{A}_{\mathrm{n}}\left(l_{\mathrm{pu}}\right).$$

The 4620 bucket model supplies at the outputs the signals of two beam position monitors (Figure 3.1). Additional outputs are the absolute value of the betatron amplitude, the indication

whether a position is populated and the normalized r.m.s. beam size. They are used for the analysis of the simulation results.

3.4 Kicker action

We assume the kickers act linearly: this means they change the transverse momentum independently of the beam position. Real kickers have a certain length, resulting in parabolic trajectories. We also neglect this length and consider only the angle between the trajectories at the beginning and the end of the kickers (kick angle). Under these circumstances the superposition principle is valid and the kicker changes the complex betatron amplitude according to

$$\mathbf{A}_{\mathrm{n}}\left(l_{\mathrm{kick}}+\varepsilon\right)=\Delta\mathbf{A}_{\mathrm{n}}\left(l_{\mathrm{kick}}\right)+\mathbf{A}_{\mathrm{n}}\left(l_{\mathrm{kick}}-\varepsilon\right).$$

Without loss of generality, we assume a bunch initially moving exactly on the closed orbit trajectory $\mathbf{A}_{\mathrm{n}}\left(l_{\mathrm{kick}}-\varepsilon\right)=0$ and the place of the kicker is supposed to be $l_{\mathrm{kick}}\equiv 0$. Then the bunch motion after the kick is described by

$$x\left(l\right)=\frac{\Delta A_{\mathrm{n}}}{\sqrt{\beta\,\gamma}}\,\sqrt{\beta_{\mathrm{x}}\left(l\right)}\,\sin\left(\int_{0}^{l}\frac{d\,\xi}{\beta\left(\xi\right)}\right)\qquad\text{for}\quad l\geq 0.$$

As the kick angles are in the order of 10^{-3} rad ($\varphi_{\mathrm{kick}}\ll 1$), they are given in good approximation by the derivative of the trajectory at the place of the kicker

$$\varphi_{\mathrm{kick}}\approx\frac{d}{dl}\,x\left(l\right)|_{l=0+\varepsilon}\,,$$

resulting in the relation

$$\varphi_{\mathrm{kick}}=\left.\frac{\Delta A_{\mathrm{n}}}{\sqrt{\beta\,\gamma}}\frac{1}{\sqrt{\beta_{\mathrm{x}}\left(l\right)}}\right|_{l=0+\varepsilon}.$$

The trajectory has to be continuous at the point of the kicker. Hence, the kick changes only the real part of the complex betatron amplitude:

$$\mathrm{Im}\,\Delta\mathbf{A}_{\mathrm{n}}\left(l_{\mathrm{kick}}\right)=0\qquad\text{and}\qquad\mathrm{Re}\,\Delta\mathbf{A}_{\mathrm{n}}\left(l_{\mathrm{kick}}\right)=\sqrt{\beta\,\gamma}\,\sqrt{\beta_{\mathrm{x}}\left(l_{\mathrm{kick}}\right)}\,\varphi_{\mathrm{kick}}\qquad(3.6)$$

As a kicker acts only on bunches and not on empty buckets, the simulation code has to check whether a bucket is populated before adding $\Delta\mathbf{A}_{\mathrm{n}}$ to the actual betatron amplitude value. Figure 3.4 shows this for the case of the extraction kicker.

3.5 Beam extraction

For extracting the beam a ‘1’ is supplied at the ‘bunch ejection’ input (see Figure 3.4). In the case where the bucket position is populated it will be emptied. An already empty position is not influenced. After emptying a bucket position, the code takes care to remove also the complex betatron amplitudes and bunch sizes for this bucket.

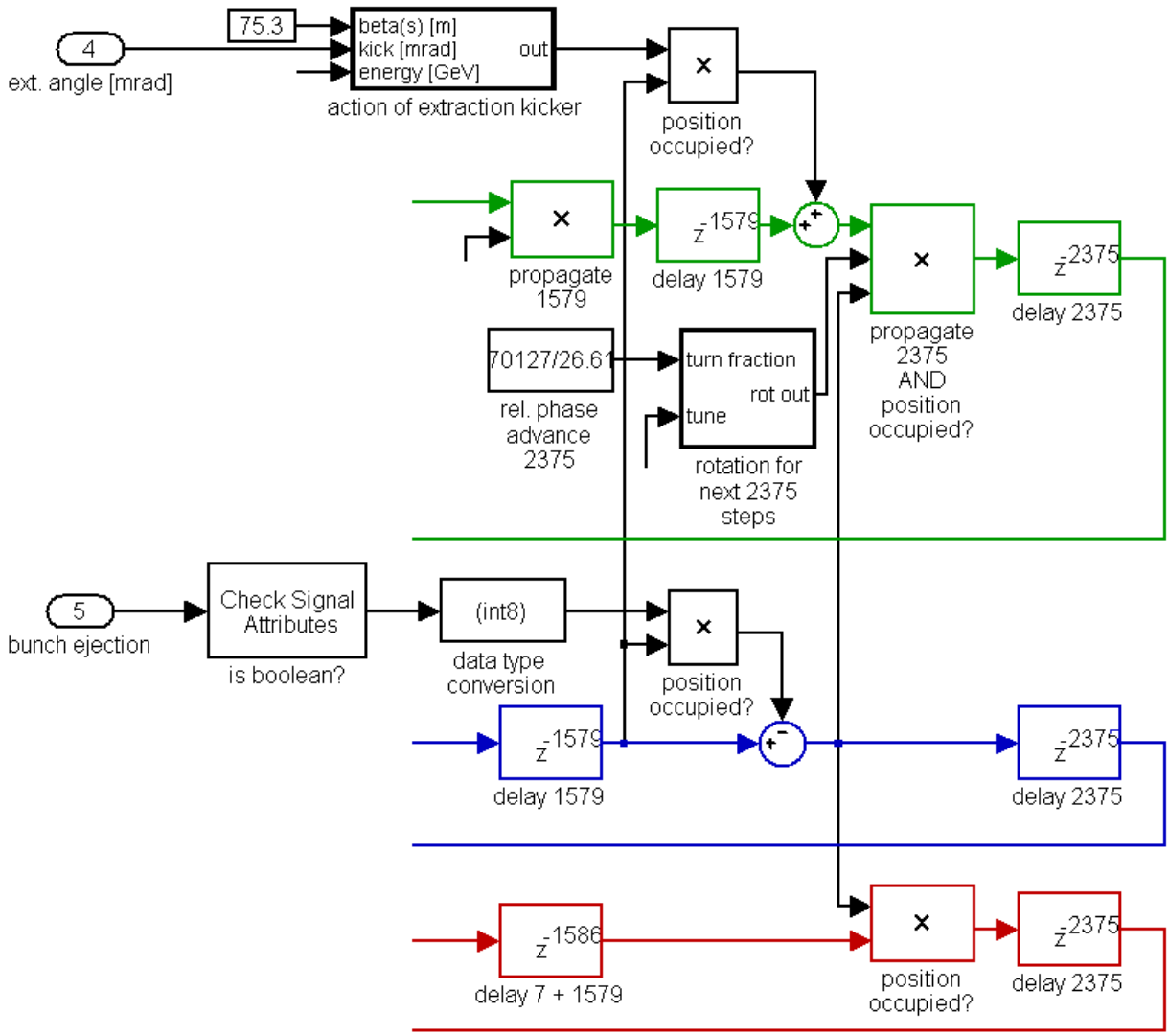

Figure 3.4: Action of extraction kicker, the kick angle value leads to a change of the betatron amplitude. The scheme of extracting bunches is also shown. All parts of the code irrelevant for the extraction are omitted.

3.6 Damper signal action

The transverse feedback kickers in the SPS are of the electrostatic type [8], i.e. they act like the beam steering system in a cathode ray tube. By impressing a voltage on two capacitor plates, enclosing the beam trajectory, an electrical field is built up, deflecting the beam.

The angle between the beam trajectory before and after the kicker φ_{kick} ($\ll 1$) is obtained from the ratio of the change of the transverse particle velocity Δv_x and the particle velocity along the accelerator $v_l = \beta\, c \approx c$

$$\varphi_{\text{kick}} = \frac{\Delta v_x}{v_l} = \frac{1}{v_l}\frac{e\, E_{\text{field}}\, L_{\text{kicker}}}{m\, v_l} \approx \frac{e\, E_{\text{field}}\, L_{\text{kicker}}}{m\, c^2}.$$

Here, E_{field} is the value of the electrical field, L_{kicker} the active kicker length, e the elementary charge, $m = \gamma\, m_{\text{p}}$ the relativistic proton mass and c the speed of light. With the particle energy

E in units of eV we obtain[3]

$$\varphi_{\mathrm{kick}} = \frac{L_{\mathrm{kicker}}}{E/e}\, E_{\mathrm{field}}.$$

Taking (3.6) into account, we obtain the conversion from the kicker field value, called 'damper signal' in the 4620 bucket model, to the change of the complex betatron amplitude

$$\mathrm{Im}\,\Delta\mathbf{A}_{\mathrm{n}}\left(l_{\mathrm{kick}}\right) = 0 \qquad \text{and} \qquad \mathrm{Re}\,\Delta\mathbf{A}_{\mathrm{n}}\left(l_{\mathrm{kick}}\right) = \sqrt{\beta\,\gamma}\,\sqrt{\beta_{\mathrm{x}}\left(l_{\mathrm{kick}}\right)}\,\frac{L_{\mathrm{kicker}}}{E/e}\,E_{\mathrm{field}}.$$

In the case where the bucket is populated, the result of this calculation $\Delta\mathbf{A}_{\mathrm{n}}$ is added to the complex betatron amplitude (see Figure 3.1).

3.7 Decoherence and emittance blow-up

Nonlinearities in the beam optics lead to a dependence of the betatron frequency on the betatron amplitude, quantified by the tune spread ΔQ. Hence, a bunch oscillating around the closed orbit shreds into filaments. In phase space, the bunch centre describes a spiral trajectory towards the origin. At the same time the average phase space density decreases. This is externally observable as a decay of the betatron amplitude and increasing bunch size. The decay time τ_{dc} (decoherence time) of the betatron amplitude is within 10% [5]

$$\frac{\tau_{\mathrm{dc}}}{T_{\mathrm{rev}}} \approx \frac{1}{\Delta Q}.$$

T_{rev} is the revolution time. For initial betatron amplitudes $A_{\mathrm{n},0}$ smaller than the r.m.s. beam size σ_{x} the bunch size increase $\Delta\sigma_{\mathrm{x}}$ is connected with the reduction of the betatron amplitude ΔA_{n} by

$$\left(\Delta\sigma_{\mathrm{x}}\right)^2 = \frac{1}{2}\left(\Delta A_{\mathrm{n}}\right)^2. \tag{3.7}$$

Nonlinearities in the beam optics, causing decoherence, are usually spread out over the whole accelerator. In the simulation presented, we contract them to one point and reduce at this point the complex betatron oscillation amplitude as follows

$$\mathbf{A}_{\mathrm{n}} \rightarrow \mathbf{A}_{\mathrm{n}}\left(1 - \frac{T_{\mathrm{rev}}}{\tau_{\mathrm{dc}}}\right).$$

According to (3.7) the beam size increases:

$$\sigma_{\mathrm{x}} \rightarrow \sigma_{\mathrm{x}} + \frac{1}{\sqrt{2}}\,\left|\mathbf{A}_{\mathrm{n}}\right|\,\frac{T_{\mathrm{rev}}}{\tau_{\mathrm{dc}}}$$

These expressions are implemented in the 'amplitude reduction ...' block (Figure 3.1).

The upper limit of the error in the betatron amplitude $|\mathbf{A}_{\mathrm{n}}|$, received by condensing the beam optic nonlinearities to one point, is in the order of $T_{\mathrm{rev}}/\tau_{\mathrm{dc}}$. For decoherence times of several hundred turns and more, this error is negligible.

The condition $A_{\mathrm{n},0} < \sigma_{\mathrm{x}}$, for the validity of (3.7) requires more attention. Initial betatron oscillation amplitudes after injections, or in our case after disturbing kicks, show values up to $4\sigma_{\mathrm{x}}$. Without countermeasures, such large initial betatron oscillation amplitudes lead to doughnut shaped phase space distributions. For such distributions one may reconsider whether r.m.s. values describe well the bunch dimensions.

[3] note $[\varphi_{\mathrm{kick}}] =$ rad, $[E_{\mathrm{field}}] =$ V, $[E] =$ eV and $[L_{\mathrm{kicker}}] =$ m

However, when the beam oscillations are damped with a feedback system, we will no longer obtain doughnuts if the damping time due to the feedback is smaller than the decoherence time $\tau_{\mathrm{fb}} < \tau_{\mathrm{dc}}$. This condition is usually fulfilled by a feedback system in normal operation. Only the part of an initial betatron amplitude not damped by the feedback $\Delta A_{\mathrm{n,dc}}$ leads to an emittance dilution [5, 6]. It is given by

$$\Delta A_{\mathrm{n,dc}} = \Delta A_{\mathrm{n},0} \frac{\tau}{\tau_{\mathrm{dc}}} \qquad \text{with} \qquad \frac{1}{\tau} = \frac{1}{\tau_{\mathrm{fb}}} + \frac{1}{\tau_{\mathrm{dc}}}.$$

Hence, the condition $A_{\mathrm{n},0} < \sigma_{\mathrm{x}}$ for (3.7) may be replaced by

$$\Delta A_{\mathrm{n,dc}} = \Delta A_{\mathrm{n},0} \, \frac{\tau}{\tau_{\mathrm{dc}}} < \sigma_{\mathrm{x}} \tag{3.8}$$

where a feedback system is present.

In practice, we may simply perform simulations and obtain from the results the damping time τ. With this value we find whether (3.8) is fulfilled and we can trust the determined bunch sizes.

4 Injection, extraction and residual kicks

In this chapter we describe the 'initializing' blocks of the simulation, see Figures 2.1 and 4.1. These provide the CNGS filling pattern, signal pattern for the extraction and the residual kicks on the second batch.

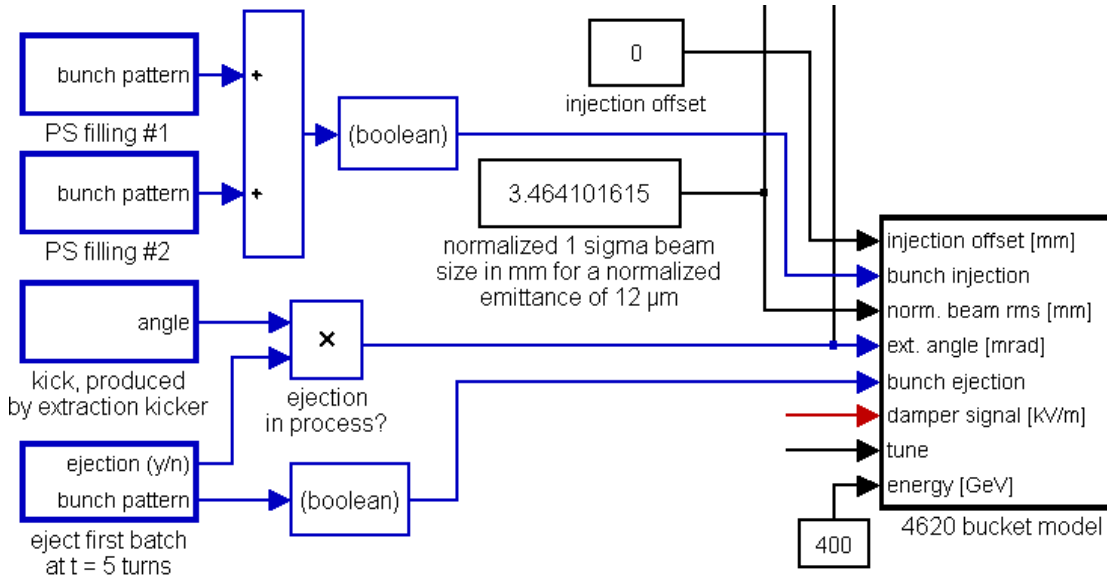

Figure 4.1: Blocks providing the time-dependent signals for injecting the CNGS fill pattern into the '4620 bucket model', as well as the signals for extraction and the residual extraction kicks on the unextracted batch.

The blocks, shown in Figure 4.1, are composed from the Simulink library blocks 'N-Sample Switch', subsystem blocks for up-sampling, and suitable delay blocks. In the block 'kick, produced ...', the measured shape of the extraction kicker strength is imported by the Simulink library function 'From File'[1]. Simulink creates an interpolation function out of the imported data and samples it with the specified sampling rate. In our case, the sampling rate is 4620 per turn.

The first two curves in Figure 4.2 show the output of the two blocks 'PS filling ...', representing the injection of the two CNGS batches, each with 2100 bunches and the nominal gaps of 210 empty bunch positions in between. For simplicity, we chose the origin of time so that the first bunch of the first batch is measured by beam position monitor no 1 at the times 1, 2, 3 and so forth. Hence, the batches have to be injected some time earlier, considering the propagation time between injection and monitor no 1.

In contrast to the real accelerator, we inject at 400 GeV and start the extraction five revolutions later. The signals controlling this process are adjusted in such a way that they hit the correct bucket positions at the extraction kicker position (third and fourth curve in Figure 4.2).

[1]The Simulink library function 'From File' reads only Matlab files with the extension '.mat'. Therefore, we first imported the measured x-y-data as a comma-separated values file into the Matlab workspace, transposed it and saved the result in the Matlab format.

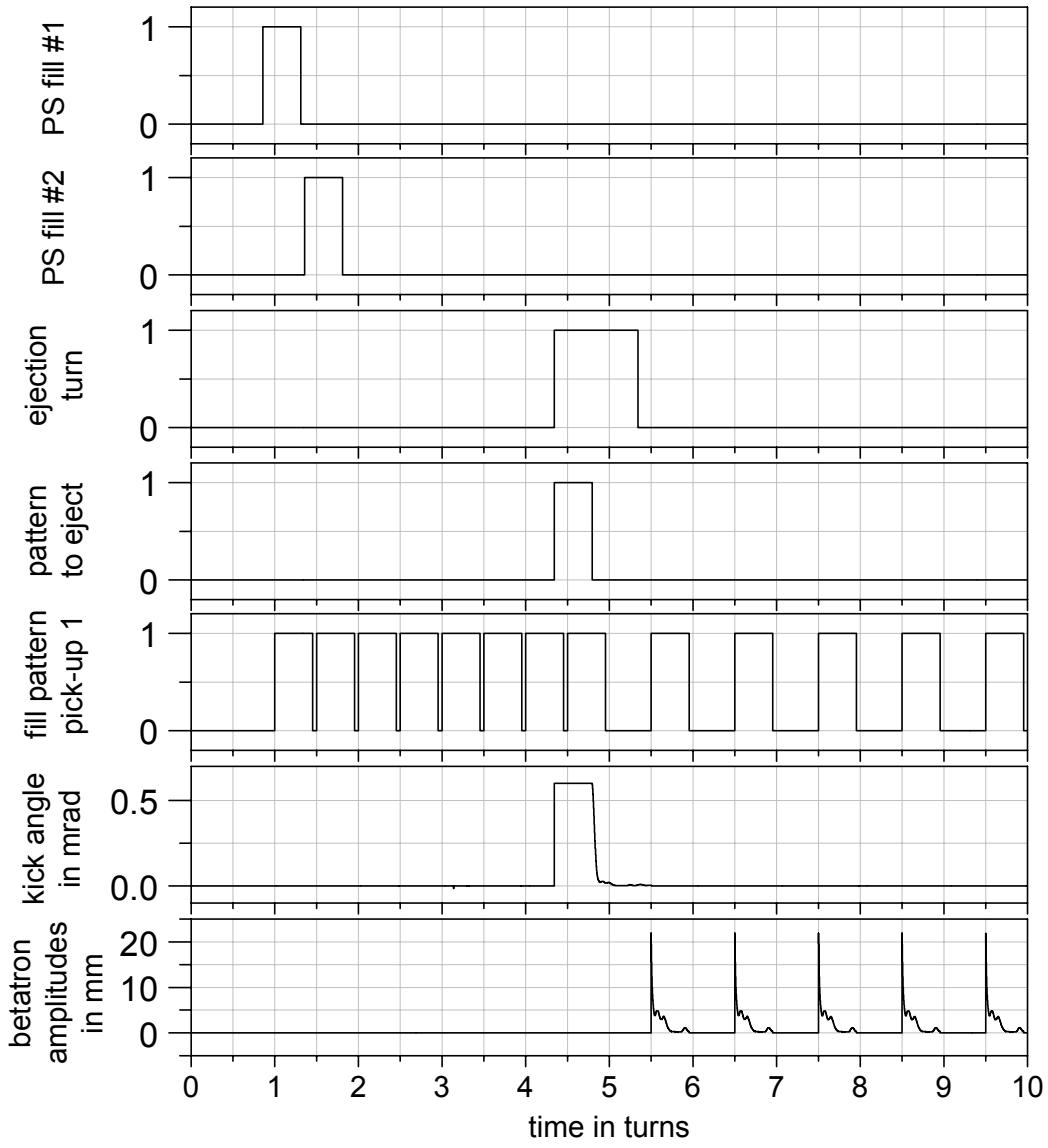

Figure 4.2: The time-dependent signals of the simulation, needed for injection and extraction. The kick angle and the betatron oscillation amplitudes, caused by the extraction kicker, are also shown. The flight times between the accelerator elements have to be taken into account. They lead to the differences in the times between the signals for injection and extraction and the signals at the monitor position.

The fifth curve shows the bucket population measured at the position of beam position monitor 1. This is the output ‘pos occ @ pu1’ of the 4620 bucket model (Figure 3.1).

Finally, the last two lines show the kick angle produced by the extraction kicker, represented by the output of ‘kick, produced ...’ and the absolute value of the betatron oscillation amplitude, ‘beta amp @ pu1’. The shape presented of the extraction kick is from a first data set, obtained from laboratory measurements [9]. We will later discuss different shapes in more detail.

5 Transverse feedback

In this chapter, the main components of the transverse bunch-by-bunch feedback system in the SPS and its modelling in our simulation are described (Figure 5.1).

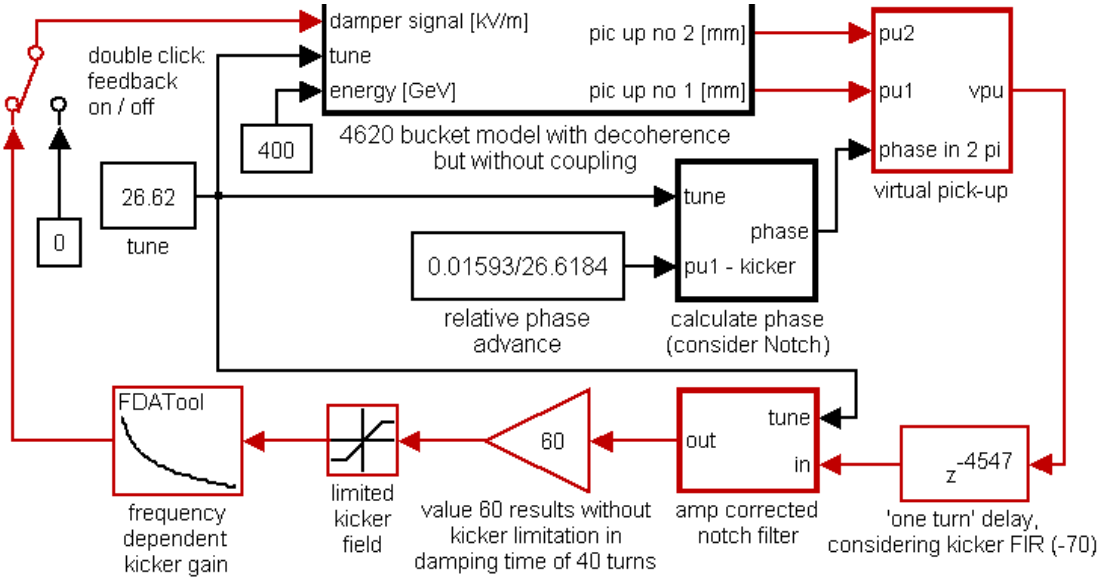

Figure 5.1: Blocks describing the behaviour of the transverse bunch-by-bunch feedback system in the SPS.

The first section contains some more general considerations. Even when they may appear well known, they are necessary to derive the expressions for the calculation of the optimal feedback phase in the third section. The second section describes notch filtering and the fourth the frequency dependence of the final stage amplifier for the feedback kicker, together with its power limitations.

5.1 General working principle of a transverse feedback

We recall a driven, damped harmonic oscillator, treated in classical theory of mechanics. Without loss of generality, we use the longitudinal coordinate l instead of the time t as a free variable, in order to obtain an analogy with the formulations in section 3.1. In the same way, $q_0 = Q/R$ is the oscillator eigenfrequency with $[q_0] = 1/\mathrm{m}$ instead of $[\omega_0] = 1/\mathrm{s}$. $2\pi R$ is the length of the particle orbit. D is the damping constant of the oscillator. The differential equation is then given by

$$\frac{1}{q_0^2}\frac{d^2}{dl^2}\,x_\mathrm{r}\,(l) + \frac{2\,D}{q_0}\frac{d}{dl}\,x_\mathrm{r}\,(l) + x_\mathrm{r}\,(l) = K_\mathrm{p}\,x_\mathrm{e}\,(l)\,,$$

with the 'time' function of the excitation $x_{\mathrm{e}}\,(l)$ and the response function of the oscillator $x_{\mathrm{r}}\,(l)$. We apply the Laplace transform [10]

$$f\,(s) = \int_0^\infty dl\; e^{-s\,l}\; f\,(l)$$

and obtain

$$\frac{1}{q_0^2}\; s^2\; x_{\mathrm{r}}\,(s) + \frac{2\;D}{q_0}\; s\; x_{\mathrm{r}}\,(s) + x_{\mathrm{r}}\,(s) = K_{\mathrm{p}}\; x_{\mathrm{e}}\,(s)\,.$$

The ratio $\frac{x_{\mathrm{r}}(s)}{x_{\mathrm{e}}(s)}$ is called the transfer function, in our case it is given by

$$G\,(s) = \frac{x_{\mathrm{r}}\,(s)}{x_{\mathrm{e}}\,(s)} = \frac{K_{\mathrm{p}}}{1 + \dfrac{2\;D}{q_0}\; s + \dfrac{1}{q_0^2}\; s^2}.$$

In control theory [11], it is represented by a block in a block diagram, Figure 5.2. From the

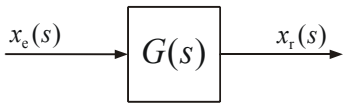

Figure 5.2: Block representing the transfer function $G\,(s)$.

transfer function we obtain with $|G\,(i\;q)|$ the amplitude response and from $\arg\,(G\,(i\;q))$ the phase response of the driven oscillator. Both graphs printed together represent the 'Bode plot' of the oscillator, shown in Figure 5.3.

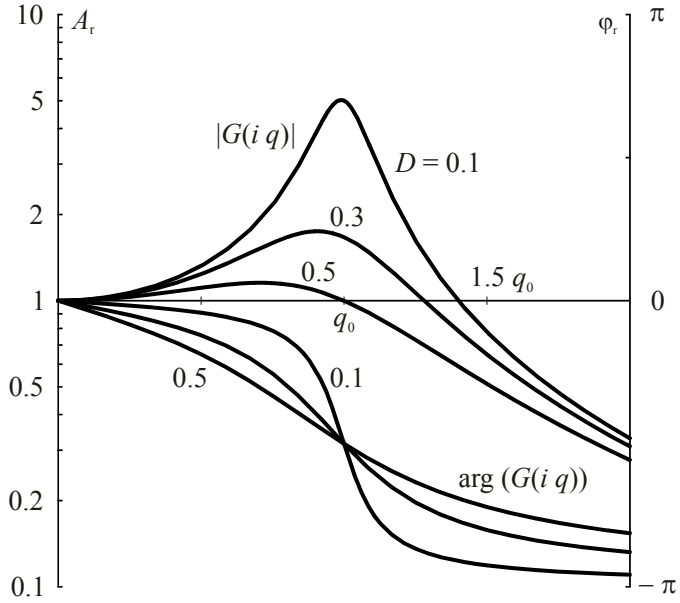

Figure 5.3: Bode plot of a driven, damped harmonic oscillator.

For small damping values D we find that the oscillator responds with the largest amplitude in the case where we excite it with $q \approx q_0$. The phase advance between oscillator response and excitation is -$\pi/2$, i.e. the oscillator follows the excitation with -$\pi/2$ (see Figure 5.4).

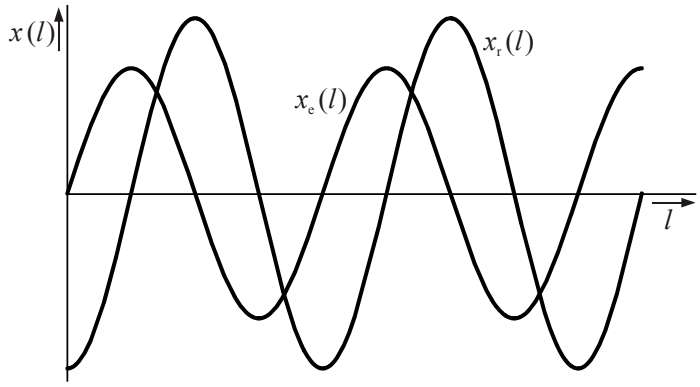

Figure 5.4: Time response of a damped harmonic oscillator on an harmonic excitation.

To reduce the amplitude response to an excitation, we have to increase the damping value D. For this, we add an additional damping value D_{fb} to D and obtain the differential equation

$$\frac{1}{q_0^2}\frac{d^2}{dl^2}\,x_{\mathrm{r}}\,(l) + \frac{2\;(D + D_{\mathrm{fb}})}{q_0}\frac{d}{dl}\,x_{\mathrm{r}}\,(l) + x_{\mathrm{r}}\,(l) = K_{\mathrm{p}}\,x_{\mathrm{e}}\,(l)\,,$$

rearranged

$$\frac{1}{q_0^2}\frac{d^2}{dl^2}\,x_{\mathrm{r}}\,(l) + \frac{2\,D}{q_0}\frac{d}{dl}\,x_{\mathrm{r}}\,(l) + x_{\mathrm{r}}\,(l) = K_{\mathrm{p}}\left(x_{\mathrm{e}}\,(l) - \frac{2\,D_{\mathrm{fb}}}{K_{\mathrm{p}}\,q_0}\frac{d}{dl}\,x_{\mathrm{r}}\,(l)\right).$$

By the negative feedback of the differentiated response signal to the excitation signal with gain $g = \frac{2\,D_{\mathrm{fb}}}{K_{\mathrm{p}}\,q_0}$, we obtain additional damping. By changing the feedback gain g we are able to adjust the additional damping constant D_{fb}. This is the common principle of all differential feedback loops (Figure 5.5).

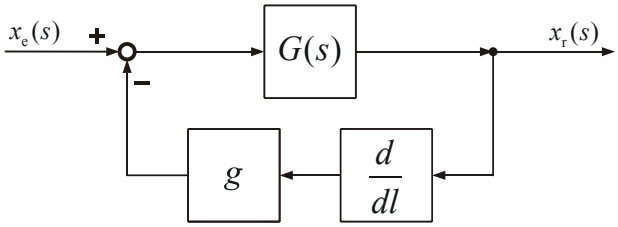

Figure 5.5: Block diagram of differential feedback loop.

This principle can be implemented directly when the response signal $x_{\mathrm{r}}\,(l)$ is measured continuously or at least with a sampling frequency larger than the eigenfrequency. Then the derivative of $x_{\mathrm{r}}\,(l)$ can be determined.

To restrict the technical effort, a transverse coupled bunch feedback measures the deviation of the beam from the closed orbit at only one position and calculates from this information a correction supplied by a feedback kicker at a second position. Between two subsequent samples, a bunch performs several betatron oscillations. Its oscillation frequency $q_0 = Q/R$ is given by the tune, in units of the revolution frequency $\omega_0 = Q\;\omega_{\mathrm{rev}}$. The information obtained is not sufficient to determine the derivative. Hence, the principle described has to be modified as follows:

In the case where the bunch oscillates with Q, a -$\pi/2$ phase shifted signal of $x_\mathrm{r}\,(l)$ corresponds to the negative derivative. Such a phase shift may be realized by installing the beam position monitor and the feedback kicker with a difference of $\left(\mathrm{integer}+\frac{1}{4}\right)$ betatron oscillations in between (Figure 5.6). The derivative is replaced by a suitable delay. An essential point

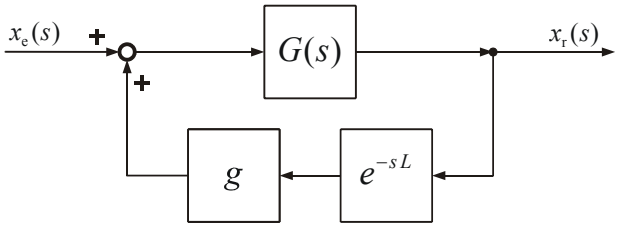

Figure 5.6: 'Time delay' feedback loop, with a delay of $L=\frac{2\pi}{q_0}\left(\mathrm{integer}+\frac{1}{4}\right)$.

is that for a delay there is no restriction for the ratio between the sample frequency and the oscillation frequency.

Such replacements are at the expense of stability. If the eigenfrequency differs from the frequency $\frac{2\pi}{L}\left(\mathrm{integer}+\frac{1}{4}\right)$, used for the delay, the response $x_\mathrm{r}\,(l)$ is damped less. For large differences, the system becomes unstable. Examinations within this scope are the subject of the Nyquist stability criterion [10, 11]: In the case of a digital bunch-by-bunch feedback system, we have to consider the interplay of a time-continuous system, represented by the beam and the feedback which is discrete in time. Instead of dealing with the Laplace transformations we have to deal with z-transformations, used for stability considerations at digital control loops [10, 11]. In practice larger excursions of the tune are avoided so that a response similar to the ideal one (described by Figure 5.5) is always obtained. We will not further discuss this subject in depth here.

For the multi bunch case, we have to ensure that the individual bunch signals are applied to the bunches that caused them. For this, we need a 'one turn delay', composed of an electronic FIFO buffer. By adjusting the depth of the FIFO buffer, signal propagation times through cables, filters and power amplifiers, together with the time of flight of the bunches, are taken into account.

5.2 Notch filter

In a transverse bunch-by-bunch feedback system the beam position monitor measures the transverse beam position. The monitor zero value for the beam position is usually calibrated once. Accelerator operation requires some freedom in laying down the beam orbit, i.e. a feedback system must not kick the beam in case the closed orbit is not at the zero position of the beam position monitor. An elegant and easy to implement way to suppress constant offsets is to subtract the previous value from each determined bunch position. This is the working principle of a periodic notch filter, shown in Figure 5.7. This filter suppresses 100% constant offsets but lets every oscillation pass, as with betatron oscillation.

Such a filter is a classical example of a digital finite impulse response filter [12]. To examine its behaviour, we set up the overall z-transfer function, deduced from Figure 5.7

$$G\,(z)=1-z^{-1}.$$

The amplitude response of the filter can be obtained from $\left|G\left(e^{i\,\Omega}\right)\right|$ and the phase response from $\arg\left(G\left(e^{i\,\Omega}\right)\right)$. In these expressions, Ω is the frequency in units of the sample frequency

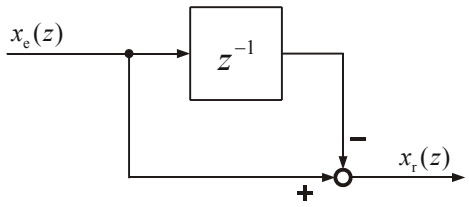

Figure 5.7: Block diagram of a notch filter. In a bunch-by-bunch feedback we have to queue the bunch values to guarantee the value of a bunch is subtracted by the value from the same bunch one revolution earlier.

f_s and $\Omega = \omega\, T = \omega / f_s$ respectively. The position of a bunch is sampled once per revolution. Hence, the sample frequency is the revolution frequency $f_s = f_{rev}$.

With

$$G\left(e^{i\,\Omega}\right) = 1 - e^{-i\,\Omega} = e^{-i\,\omega/2}\left(e^{i\,\Omega/2} - e^{-i\,\Omega/2}\right) = 2\,i\,e^{-i\,\Omega/2}\sin\frac{\Omega}{2} = 2\,e^{i(\pi-\Omega)/2}\sin\frac{\Omega}{2}$$

the amplitude and phase response of a periodic notch filter are

$$\begin{aligned}\left|G\left(e^{i\,\Omega}\right)\right| &= 2\left|\sin\frac{\Omega}{2}\right| \\ \arg\left(G\left(e^{i\,\Omega}\right)\right) &= \frac{\pi-\Omega}{2} + \arg\left(\sin\frac{\Omega}{2}\right).\end{aligned}$$

If the bunch is oscillating, the input value x_e of the periodic notch filter oscillates with the betatron frequency. The tune Q is the betatron frequency in units of the revolution frequency. With $\Omega = 2\pi\, Q$ we obtain the response of a periodic notch filter within the transverse feedback chain

$$\begin{aligned}A_r\left(Q\right) &= 2\left|\sin\pi Q\right| \\ \varphi_r\left(Q\right) &= \pi\left(\tfrac{1}{2} - Q\right) + \arg\left(\sin\pi Q\right),\end{aligned}$$

shown in Figure 5.8.

A periodic notch filter changes the absolute values of the measured bunch positions and the phasing. The latter has to be taken into account in the adjustment of the phase difference between beam position monitor and feedback kicker. We will come back to this point in the next section.

At the SPS first the working point (tune) is chosen. Then an analog amplifier in front of the ADCs is usually adjusted for the beam signals, so that the whole digital dynamic range of the feedback system is used. This treatment corresponds to an amplitude correction of the notch output depending on the actual tune value:

$$x_r \rightarrow \frac{x_r}{2\sin\left(\pi\ \text{fractional part}\, Q\right)}.$$

In our simulation we implemented the notch filter using a ‘one turn’ delay with z^{-4620}, so that each bunch value hits the value from the same bunch after one turn. In addition, the amplitude correction of the value is also applied in the block ‘amp corrected notch filter’ (Figure 5.1).

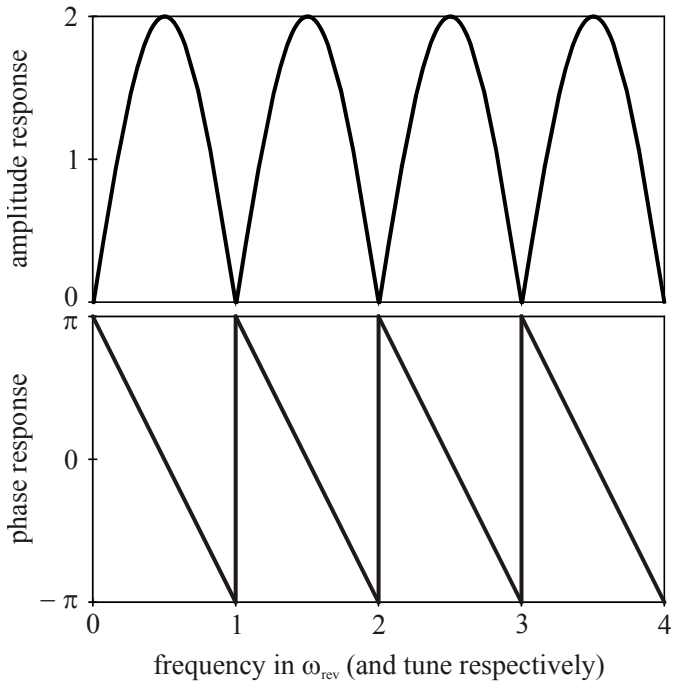

Figure 5.8: Amplitude and phase response of a periodic notch filter within the chain of a transverse feedback.

5.3 Virtual pick-up and optimal feedback phase

In practice we do not want to adjust the distance between the beam position monitor (pick-up) and the feedback kicker each time we change the tune. By the use of two monitors, placed at a distance of about $\pi/2$ betatron phase advance in between, the phasing between the measured bunch signal and the kicker signal can be adjusted [**?**].

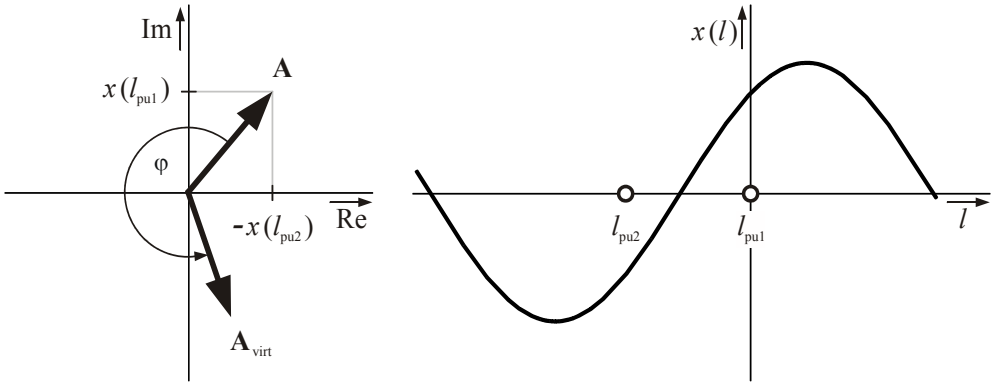

Figure 5.9: Pointer diagram, showing the generation principle of a virtual monitor signal from two monitor signals with $\pi/2$ betatron phase advance in between.

For explanation, Figure 5.9 shows the complex angular pointer (3.4), describing a betatron oscillation

$$x\,(l) = \mathrm{Im}\left(\mathbf{A}\, e^{i\, q_0\, l}\right).$$

If $x\,(l_{\mathrm{pu2}})$ and $x\,(l_{\mathrm{pu1}})$ are the measured beam deviations at the monitor positions l_{pu2} and l_{pu1},

we can reconstruct the complex angular pointer at the position l_{pu1} with

$$\mathbf{A} = -x\left(l_{\mathrm{pu2}}\right) + i\, x\left(l_{\mathrm{pu1}}\right).$$

Combining both signals we can produce a signal having a phase advance of φ with respect to l_{pu1}. This corresponds to a rotation of $\mathbf{A}$ in the complex plane $\mathbf{A}_{\mathrm{virt}} = \mathbf{A}\, e^{i\,\varphi}$. The shifted signal follows from

$$x\left(l_{\mathrm{virt}}\right) = \mathrm{Im}\left(\mathbf{A}\, e^{i\,\varphi}\right) = -x\left(l_{\mathrm{pu2}}\right)\ \sin\varphi + x\left(l_{\mathrm{pu1}}\right)\ \cos\varphi. \tag{5.1}$$

As the same signal would be obtained from a monitor with a betatron phase advance of $-\varphi$ with respect to monitor no 1, one can think of the signal coming from a virtual pick-up.

Now, we determine the optimal phase φ for the feedback, considering the phase advance of monitor no 1 and kicker one revolution later as well as the phase advance through the notch filter, so that we obtain an over all phase advance of $-\pi/2$

$$\frac{\varphi}{2\pi} = \mathrm{fractional\,part}\left(\frac{\Psi\left(l_{\mathrm{kick}}\right) - \Psi\left(l_{\mathrm{pu1}}\right)}{2\pi} + Q + \underbrace{\frac{\mathrm{fractional\,part}\, Q}{2} - \frac{1}{4}}_{\text{notch filter correction}} + \frac{3}{4}\right).$$

In our simulation, we use the approximation (3.3) and implement in the block ‘calculate phase’ (Figure 5.1) the expression

$$\frac{\varphi}{2\pi} = \mathrm{fractional\,part}\left(\left(\frac{\Psi_{\mathrm{mad}}\left(l_{\mathrm{kick}}\right) - \Psi_{\mathrm{mad}}\left(l_{\mathrm{pu1}}\right)}{2\pi\, Q_{\mathrm{mad}}} + 1\right)\, Q + \frac{\mathrm{fractional\,part}\, Q}{2} + \frac{1}{2}\right). \tag{5.2}$$

Using the determined value, the block ‘virtual pick-up’ generates the virtual signal according to (5.1). The block also takes into account that $x\left(l_{\mathrm{pu2}}\right)$ is measured earlier than $x\left(l_{\mathrm{pu1}}\right)$, and compensates this by a delay.

5.4 Behaviour of final stage amplifier

In this section, we will discuss the behaviour of the final stage amplifier, driving the feedback kicker. When describing the behaviour of the amplifier, we always mean the combination of amplifier and kicker which loads the amplifier capacitively.

Without additional measures, a final stage amplifier with phase distortion at its frequency band limit may lead to unstable behaviour of the feedback loop. This is due to the fact that the signal propagation time through the amplifier depends on the signal frequency. Such effects are well known in control theory [10]. Here, we will briefly show the consequences for different modes of coupled bunch oscillations.

In the case of the SPS, the low-pass characteristic of the amplifier is quite well described by a first order low-pass. For unity gain, its transfer function is

$$G_{\mathrm{LP}}\left(s\right) = \frac{1}{1 + \frac{s}{2\pi f_{\mathrm{3dB}}}},$$

with Bode plot as shown in Figure 5.10.

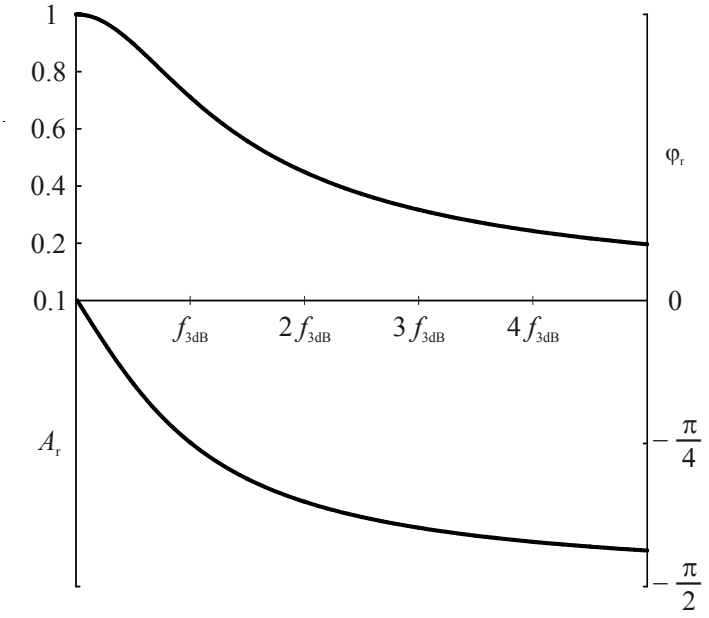

Figure 5.10: Bode plot of a first order low-pass filter, as the most simple description of the power amplifier frequency response.

The amplitude of a harmonic input signal with frequency $f_{3\mathrm{dB}}$ is reduced at the output to $1/\sqrt{2}$. Essential for the stability of our feedback is the phase response. The signal propagation time (group delay) through the amplifier is given by the derivative of the phase response

$$T_{\mathrm{sig}}(f) = -\frac{1}{2\pi}\frac{d}{df}\arg\left(G\left(i\,2\pi f\right)\right), \tag{5.3}$$

shown in Figure 5.11. High frequency signal components propagate faster through a low-pass than low frequency ones.

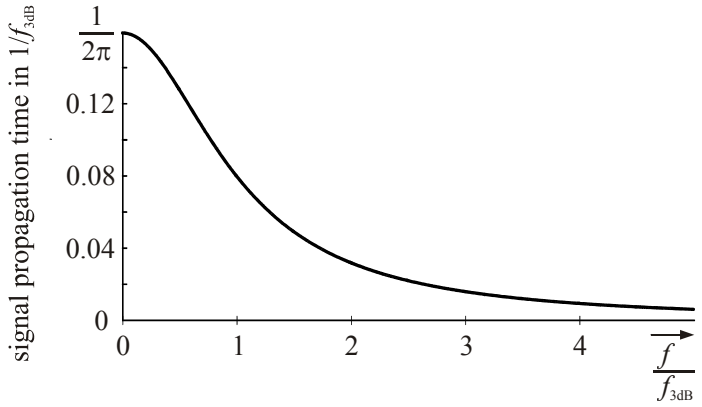

Figure 5.11: Signal propagation time through a low-pass.

What are the consequences for a feedback? Assume an accelerator filled with a batch of bunches in one half of the ring. Further, these bunches are coupled and perform coupled bunch oscillations. We measure the bunch positions with the beam position monitor. This may result in a slowly oscillating signal, propagating through the feedback from the monitor to the kicker. For the case without 'one turn' delay, Figure 5.12a shows the initial monitor signal and the final signal at the kicker. Due to the low-pass characteristics of the final stage amplifier, the

signal is delayed, deformed and the amplitude reduced. For feedback, we adjust the delay between monitor and kicker to be such that the kicker signal covers the batch (Figure 5.12b). This requires a delay value of one turn minus the signal propagation time through the amplifier. In the case shown, the bandwidth of the amplifier is $f_{3\mathrm{dB}} = 5 f_{\mathrm{rev}}$, resulting in an delay of $(1 - 0.0287)\ T_{\mathrm{rev}}$ to match both signals.

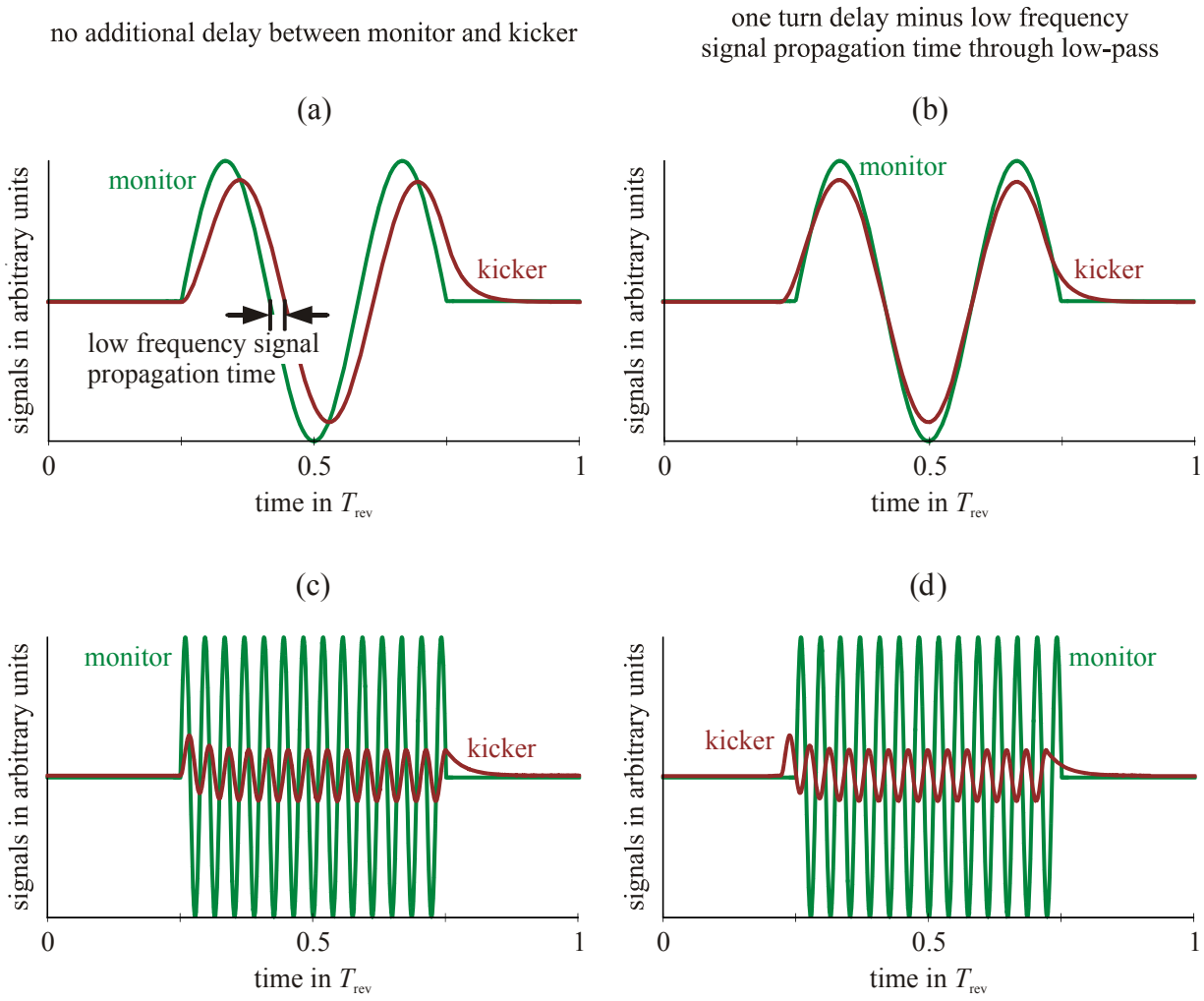

Figure 5.12: Monitor signal and signal after low-pass (kicker), for a low frequency signal before (a) and after (b) introducing a delay for matching the signals. In the case of high frequency signals (c), the use of the low frequency delay leads to a mismatch (d).

Figure 5.12c shows the monitor and kicker signals for a mode, causing a fast oscillating signal. The smaller signal propagation time is noticeable. If we use the same time delay as in the previous case, we obtain the situation shown in Figure 5.12d. The signal propagates too fast through the feedback and no longer matches the batch properly. This leads to a kicker signal exciting the beam. For damping this mode, we have to change the delay.

In the case only one unstable mode is present, it may be sufficient to adjust the delay value such that this mode will be damped. But treating impedances driving at the same time coupled bunch modes, leading to high and low frequency signals in the feedback path, requires frequency independent signal propagation times.

Additional measures are taken in front of the final stage amplifier, to achieve a *linear* overall phase response [8]. Because of (5.3) high and low frequency signals propagate then with the same speed through the amplifier.

In the SPS, the final stage amplifier is compensated in this way [8]. Therefore, in our simulation a low-pass with linear phase response beyond the 3dB point must also be used. Digital finite impulse response (FIR) filters have linear phase responses. Furthermore they fit ideally in our simulation concept. Hence, we use a FIR low-pass filter in our simulation to model the final stage amplifier including its phase compensation.

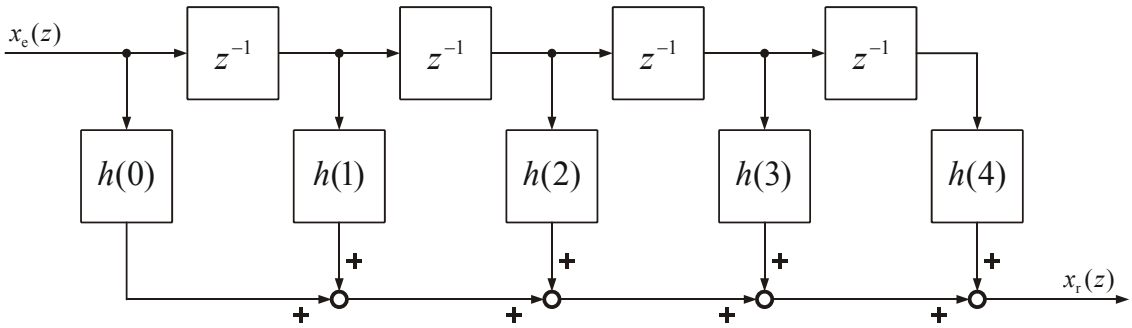

Figure 5.13: Block diagram of a finite impulse response (FIR) filter with $m = 4$.

A FIR filter, shown in Figure 5.13 for $m = 4$, adds subsequent delayed input values after multiplying them with the coefficients $h(\mu)$

$$G_{\mathrm{FIR}}(z) = \sum_{\mu=0}^{m} h(\mu)\ z^{-\mu}.$$

If we need a filter with the frequency response $G_\omega\left(e^{i\,\Omega}\right)$, then we can calculate the coefficients according to the least error square approximation [12]

$$h(k) = \frac{1}{2\pi} \int_{-\pi}^{\pi} G_\omega\left(e^{i\,\Omega}\right)\ e^{i\,\Omega\,k}\, d\Omega.$$

In Simulink, the block 'Digital Filter Design' from the DSP Blockset calculates the filter coefficients. We specify the desired amplitude response via a sufficient number of points, defining amplitude values for specific frequencies. As we use one revolution as basic time unit in the simulation it is very simple to supply the filter design tool with the normalized amplitude response.

The sampling frequency in the simulation corresponds to a real sampling frequency of $f_{\mathrm{samp}} = 4620 \times 43375.4$ Hz. We obtain a frequency spectrum from 0 to $f_{\mathrm{samp}}/2$. Dividing the 3dB frequency of the SPS feedback system (4.5 MHz) by $f_{\mathrm{samp}}/2$, results in a normalized 3dB frequency of $f_{\mathrm{n,3dB}} = 0.02246$. The required normalized amplitude response values are the values $|G_{\mathrm{LP}}(i\,2\pi f)|$ from $f = 0$ to $f = 1$ calculated with $f_{\mathrm{n,3dB}}$. Figure 5.14 shows the content of the filter design tool and the 'frequency dependent amplifier gain' block respectively of Figure 5.1. We designed a FIR filter of order 140, describing the 4.5 MHz bandwidth limitation of the SPS feedback sufficiently accurately. Figure 5.14 also shows the phase response which is linear, as discussed earlier.

If the designed filter is excited by an impulse, we obtain the maximum output signal after 70 digital steps (group delay). Consequently, this propagation time must be taken into account and the one turn delay adjusted adequately.

In addition to a lower gain for higher frequency parts, an amplifier is not able to deliver an infinite output signal. The power amplifier for the horizontal feedback kicker in the SPS is able

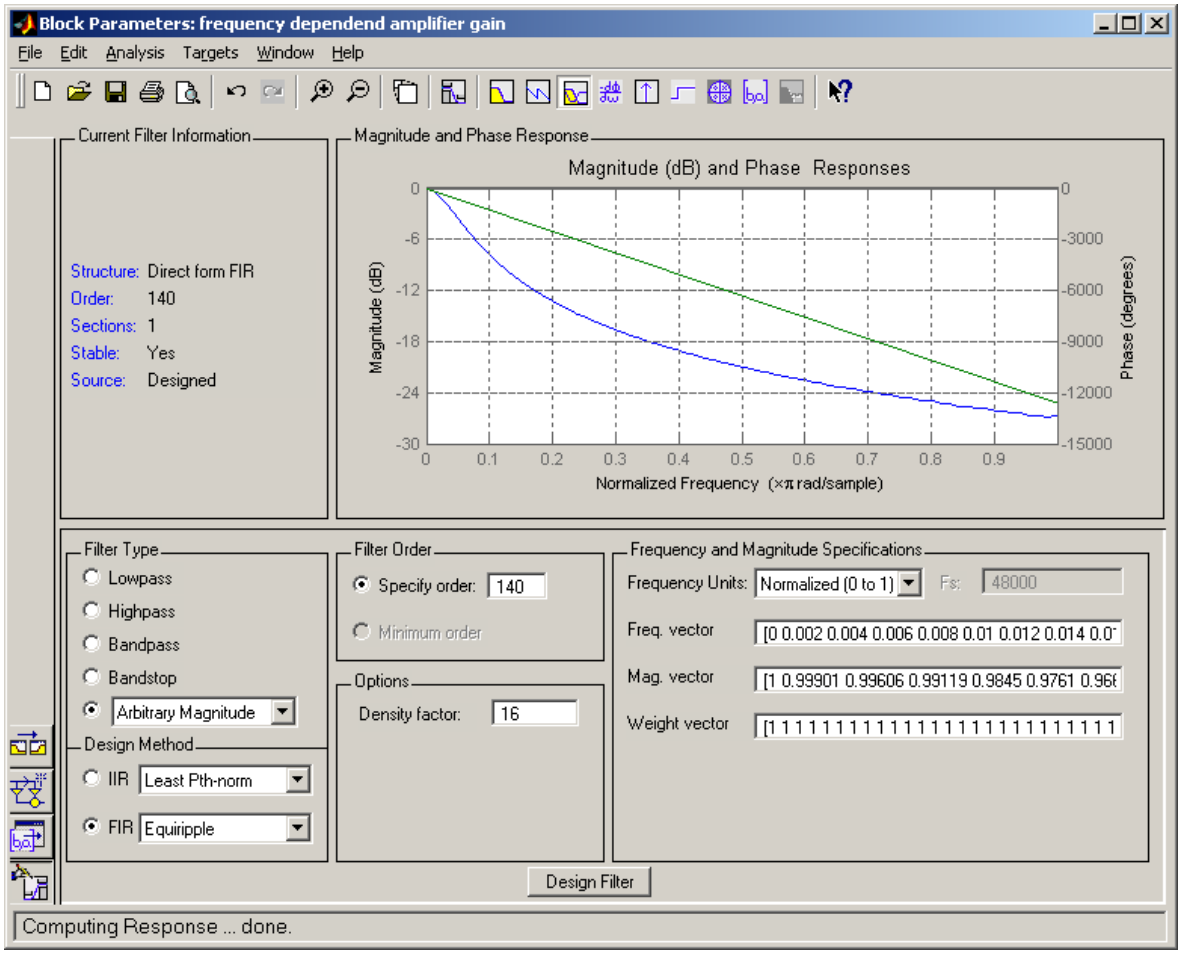

Figure 5.14: The design of the low-pass FIR filter with the filter design tool form Simulink, describing the bandwidth limitation of the SPS feedback. (For simulation used sampling frequency: 200 MHz.)

to build up an electric field of 20.42 kV/m for low frequency signals. The simplest method for modelling this effect is to use a Simulink 'saturation' block. As there is less power available for higher frequency components, the 'saturation' block has to be placed in front of the FIR low-pass filter (Figure 5.1).

5.5 Feedback gain adjustment

One of the free parameters in the simulation, as in the real system, is the feedback gain. The value used in the simulation has the units of kV/mm. It is proportional to the feedback gain, discussed in Section 5.1. The value was chosen in order to obtain a damping time between 40 and 50 turns for small betatron oscillations (amplifier not saturated).

5.6 Unconsidered feedback properties

In our simulations, we omit some properties of transverse feedbacks which are not important for the examination of the extraction of CNGS beam form the SPS in the ideal case. These are for instance small quantization effects caused by the digital signal processing and beam intensity

effects.

Quantization effects due to the digital signal processing get important for damping small betatron amplitudes. This may play an important role for the long time and noise behaviour of a transverse feedback. Here, we have large betatron oscillation amplitudes and the time of interest is short (2200 turns).

Variations in the beam intensity are in our case dominated by the injection procedure from the pre-accelerator PS and beam capture in the SPS. In the ideal case, all bunches have the same intensity and there is no population in the kicker gaps. The transverse beam position, measured by the beam position monitors are intensity dependent. This results finally in an intensity dependent feedback gain as high intense bunches lead to larger beam position values at the monitor outputs as low intense ones. In the case of the CNGS beam extraction the final stage amplifiers are operated at the saturation limit leading in any case to a hard limitation of the feedback gain. Hence, beam intensity effects are expected to be relatively small.

6 Analysis and visualization of beam parameters

Figure 6.1 shows as an example the diagnostics block '4620 bunch full damping time determination' of the upper right part of Figure 2.1. It checks bunch-by-bunch whether the actual

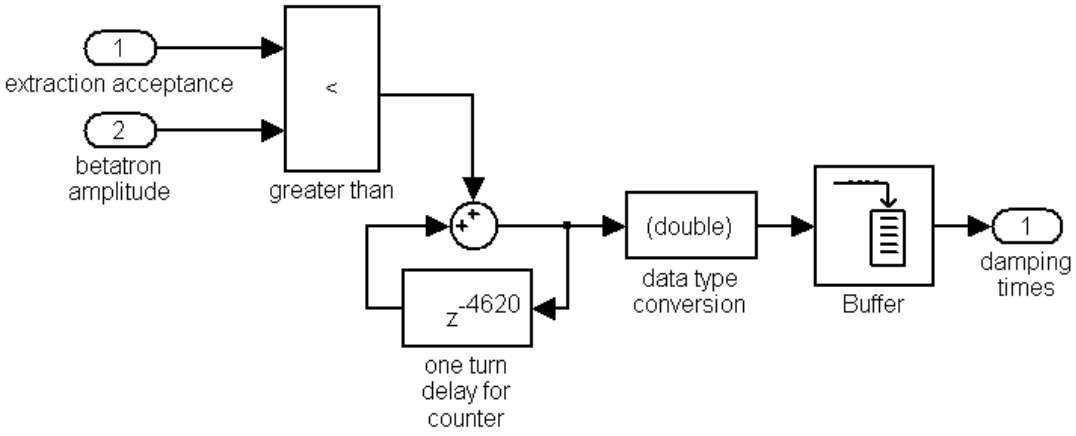

Figure 6.1: Contents of block '4620 bunch full damping time determination'. It increments turn-by-turn numbers for certain bunches in case their betatron oscillations and sizes are too large.

betatron amplitude is below the extraction acceptance for the CNGS target. If this is not the case, it increments a turn counter. At the output, it supplies a list of numbers per turn. If a number is still being incremented at a given turn during the simulation, the corresponding bunch does not fulfill the CNGS constraints at this turn. A number no longer changing indicates that the corresponding bunch fulfills the constraints.

For the constraint we implemented a maximum oscillation amplitude corresponding to 1% extraction kicker ripple at the extraction as the CNGS baseline which had recently been relaxed [14] to 1.5%. Repeating (3.6), these values are

$$\begin{aligned} A_{\mathrm{n,threshold}} &= \frac{\text{constraint}}{100\%}\sqrt{\beta\,\gamma}\,\sqrt{\beta\,(s_{\mathrm{kick}})}\,\varphi_{\mathrm{kick}} \\ A_{\mathrm{n,threshold}} &= \begin{cases} 1.073\,\sqrt{\mathrm{m}} & \text{for} \quad 1\% \quad \text{constraint} \\ 1.61\,\sqrt{\mathrm{m}} & \text{for} \quad 1.5\% \text{ constraint.} \end{cases} \end{aligned} \tag{6.1}$$

A bunch with the size σ_{x} larger than the nominal value $\sigma_{\mathrm{x,nominal}}$, has to show a smaller betatron oscillation amplitude to meet this constraints. Hence, the extraction acceptance value in Figure 6.1 is given by

$$\text{extraction acceptance} = A_{\mathrm{n,threshold}} - (\sigma_{\mathrm{x}} - \sigma_{\mathrm{x,nominal}})\,.$$

The resulting lists are exported to the Matlab worksapce for further treatment and for saving as asci files. Moreover they are also presented online via Simulink vector scopes.

In the block '4620 bunch damping time determination' we store the initial betatron amplitudes after the extraction kick and count revolutions until the betatron amplitudes are below $1/e$ of the initial amplitudes.

The block 'determine maximum relative kick ...' supplies the maximum relative kick on the second batch caused by the MKE kicker. Finally, the values obtained from 'determine initial betatron amplitude ...' are required to calculate the beam losses at the extraction septum, as discussed in the next chapter. The normalized emittances are obtained by squaring the normalized beam sizes.

The output signals from the '4620 bucket model ...' can be observed in time domain via a virtual scope, Figure 6.2. For example one can observe in the third row the betatron amplitudes, measured at the beam position monitors. The last row shows the (clipped) feedback kicker signal.

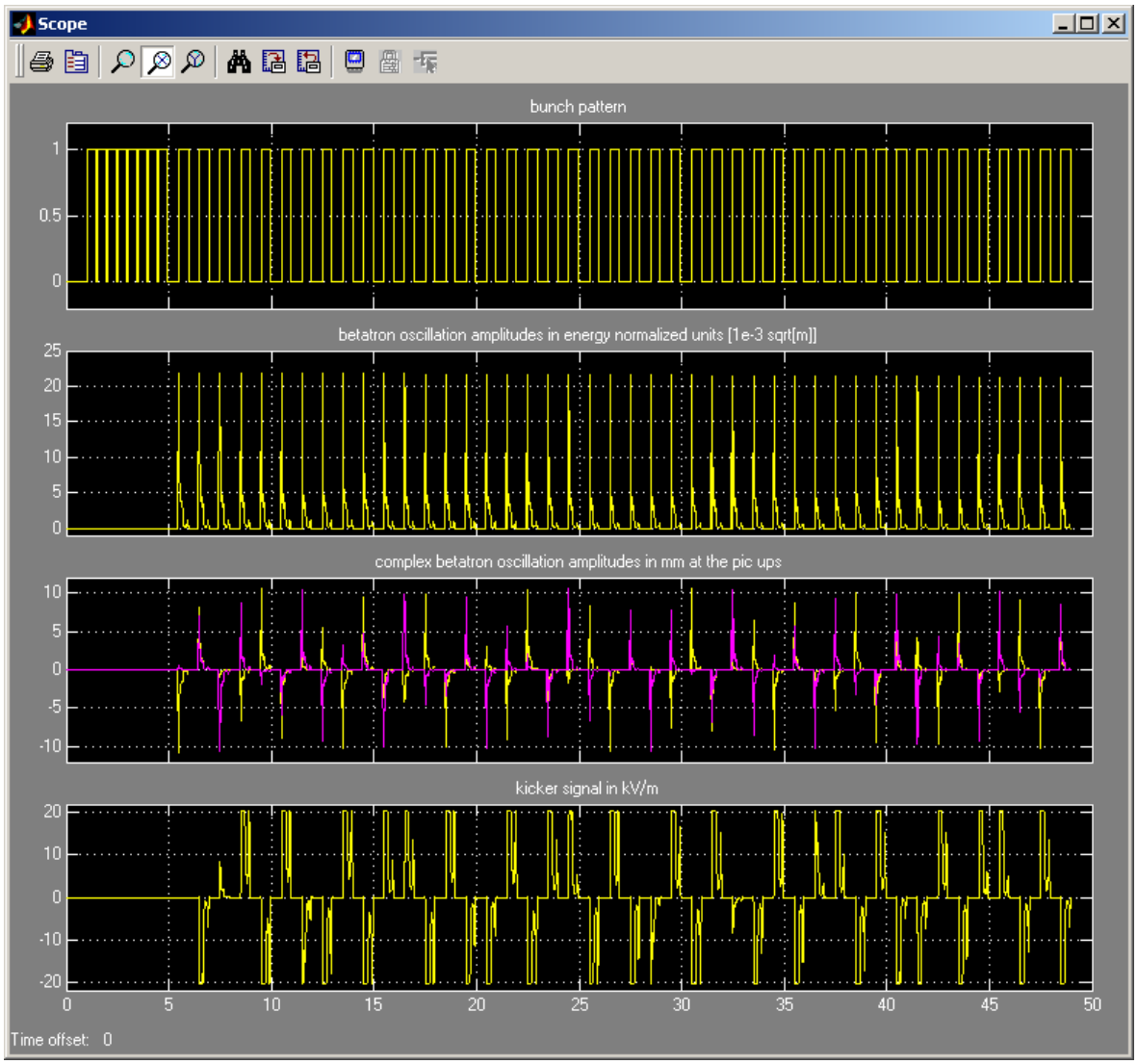

Figure 6.2: Virtual scope, showing the bunch pattern, betatron oscillation amplitudes, the beam positions at the two beam position monitors (complex betatron oscillation amplitude) and the kicker signal in kV/m. Due to damping times up to 1000 turns, the betatron oscillation amplitudes are reduced only minimally within the first 50 turns shown.

7 Considerations on beam losses

In this chapter, we summarize considerations which are important for loss evaluation during the CNGS beam extraction but do not enter the feedback model.

At extraction the beam is steered towards the septum via an orbit bump to keep the required extraction kick angle low. Therefore, the physical aperture is reduced to eight times the nominal CNGS beam size [15]. The first bunches of the second batch receive a kick from the extraction kicker, resulting in initial betatron oscillation amplitudes of about five to six times the bunch size. Hence, we obtain a remaining aperture of two to three times the beam size. Beam starts to be lost in the case of $3\,\sigma$ apertures. We should therefore examine potential beam losses at the extraction septum.

Figure 7.1a shows a bunch in phase space, with an original aperture of eight times the bunch

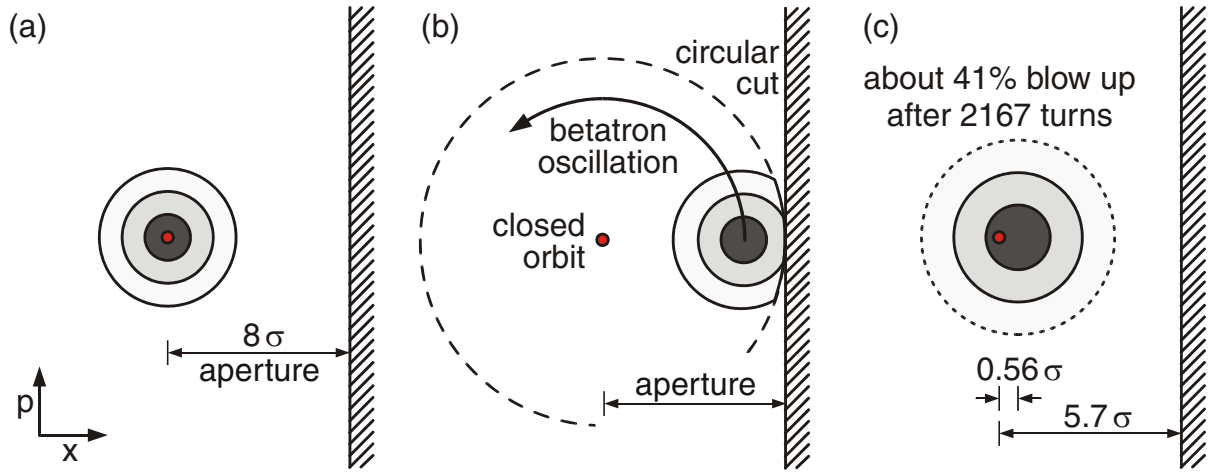

Figure 7.1: Peeling of bunch particles in phase space due to an aperture limitation in the case of large betatron oscillations.

size. This bunch is deflected by a kick, resulting in a betatron oscillation amplitude of six times the bunch size. As the extraction kick deflects the bunch directly towards the septum, all particles with coordinates larger that eight times the bunch sizes $x > 8\,\sigma$ are lost. In phase space, a straight cut was made in the bunch population. If there is no damping mechanism, the bunch centre will rotate along a circle in phase space due to the betatron oscillations. For reasonable tune values[1], we obtain a circular cut after less than 30 turns[2] (Figure 7.1b).

As we will see in the next chapter, large betatron oscillations of CNGS beam at top energy are damped by the feedback within several hundred turns. Because the time needed for all loss of particles to occur is much less (30 turns) we can estimate the total losses by calculating the losses due to circular cuts from the initial betatron amplitudes.

One may argue that the bunch size increase (blow-up) has to be taken into account and a bunch will additionally lose particles due to its growing dimension. However, the feedback damps beam oscillations faster than the beam blows up, i.e. the feedback damping time is

[1] 'reasonable' tune values are away from integer and half integer values to avoid optical resonances

[2] This may be verified by comparing the losses by one turn straight cuts and multi turn circular cuts.

Table 7.1: loss factors obtained by numerical integration for an aperture of $8\,\sigma$ as a function of initial betatron oscillation amplitudes in the case of a Gaussian density distribution

betatron oscillation amplitude in σ	relative loss for $8\,\sigma$ aperture
0	0.000
0.5	0.000
1	0.000
1.5	$1.00\ 10^{-10}$
2	$2.04\ 10^{-9}$
2.5	$3.51\ 10^{-8}$
3	$4.83\ 10^{-7}$
3.5	$5.30\ 10^{-7}$
4	$4.62\ 10^{-5}$
4.5	$3.20\ 10^{-4}$
5	$1.76\ 10^{-3}$
5.5	$7.74\ 10^{-3}$
6	$2.72\ 10^{-2}$
6.5	$7.68\ 10^{-2}$
7	0.176
7.5	0.333
8	0.527

smaller than the decoherence time. Hence, with feedback on, losses at aperture limits will only appear in the first turns after the initial kick and beam blow-up can be neglected.

This fact is illustrated in Figure 7.1c. After 2167 turns a bunch initially displaced by about $6\,\sigma$ and an aperture of $8\,\sigma$, is blown up by 41%. Due to the blow up, the aperture, in units of the beam size, decreased to $5.7\,\sigma$. The betatron oscillation amplitude decreased during the same time to $0.56\,\sigma$. Particles at $3\,\sigma$, initially touching the aperture limit are now far away from the aperture limit.

Table 7.1 was calculated by numerical integration and contains the loss factors for circular cuts as function of the initial betatron oscillation amplitude for an aperture of $8\,\sigma$. The factors obtained are confirmed by multi-particle tracking [16]. Losses given in the next chapter were obtained by interpolating between the corresponding values of Table 7.1.

8 Results obtained

In this chapter we discuss the specific results obtained for the CNGS beam at extraction. Possible improvements by having larger gaps between the two CNGS batches are also treated.

8.1 Residual kicks

As input parameter for the simulations, we used the measured shapes of the kicker strength, supplied by E. Gaxiola [9]. Figure 8.1 shows the normalized kicker pulse.

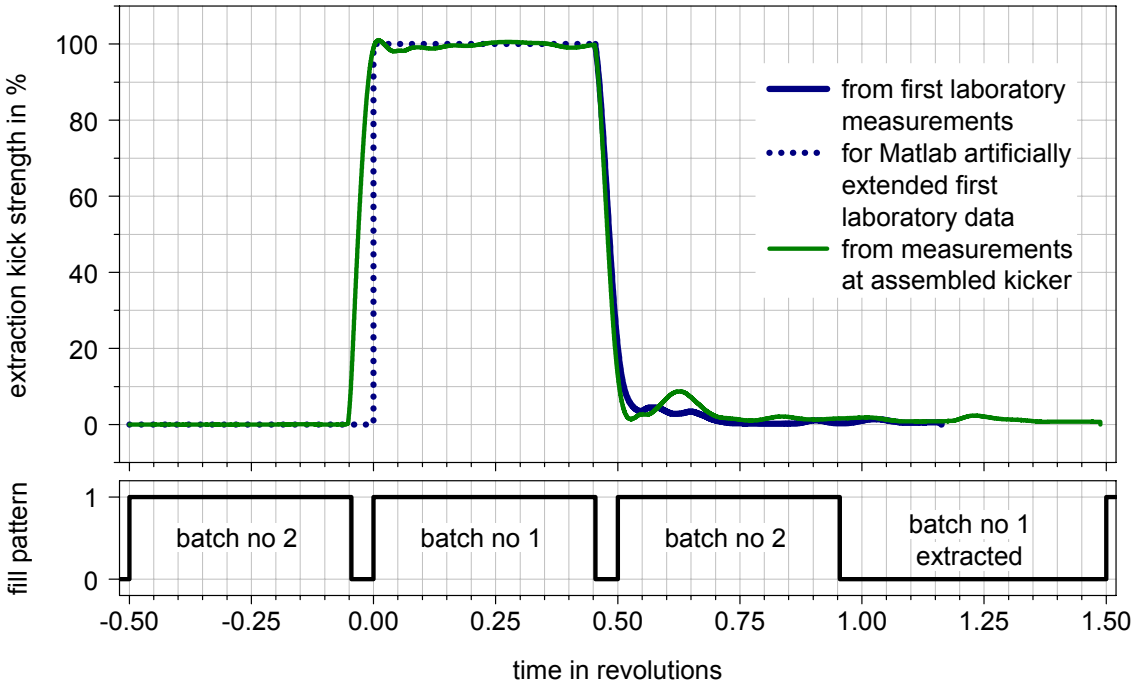

Figure 8.1: Normalized ($100\,\% = 0.6\,\text{mrad}$) measured kicker pulses and nominal fill pattern (2100 bunches per batch).

The falling edge is longer than the rising edge. Furthermore, the falling edge shows trailing ripples. Therefore, the main focus of the first measurements at a test assembly in the laboratory was the falling edge [9]. Simulations with this data consider only the falling edge. Effects caused by the rising edge can be examined using the data from the assembled kickers [9].

The CNGS target constraints can be converted into a maximum tolerable deviation of the extraction kicker field from the nominal value. The original constraint is 1 % [9, 14]. In the simulation we adjusted the timing of the kicker firing so that the first and the last extracted bunch obtain 99 % of the full kick strength. Figure 8.2 shows the residual kicks that bunches of the second batch suffer. Using the laboratory data, the first bunch of the second would obtain a kick of about 20 % of the extraction kick. This has been reduced during the final kicker assembly and adjustment to a value of about 13 %. One turn earlier, the rising edge of the extraction kick will also kick the last bunch of the second batch.

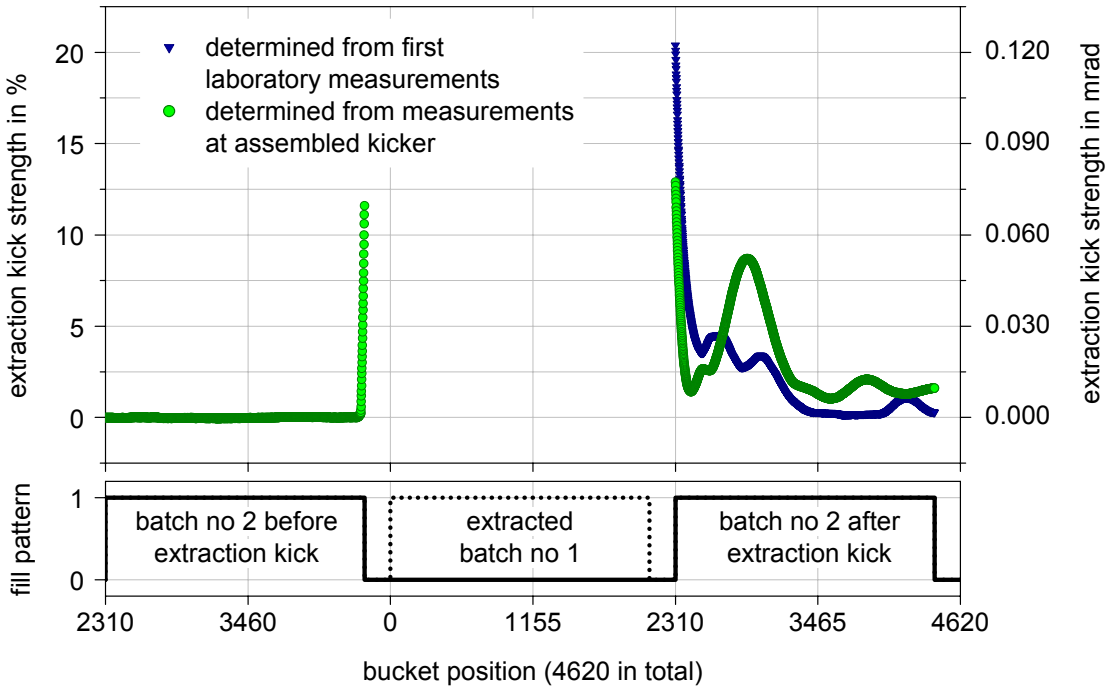

Figure 8.2: Kicks of the extraction kicker, applied to the still circulating batch at the extraction of the first batch.

8.2 Absence of feedback

The analytical approach used for the determination of the emittance blow up in Section 3.7 is not valid in case of large initial betatron amplitudes and the absence of damping with feedback. Nevertheless, the reduction of the betatron oscillation amplitude according to the decoherence time of $\tau_{\mathrm{dc}} = 10000$ turns [3] is still correct. It leads to a slow damping of the oscillations. In simulations without feedback we only checked whether the betatron oscillation amplitude is below the 1% acceptance value (6.1) for the target. In reality, the blow up reduces this limit.

Figure 8.3 shows for each bunch individually after how many turns its remaining betatron oscillation amplitude is below the 1% acceptance value. The extraction of the second batch takes place 50 ms (about 2170 turns) after the extraction of the first. For this reason, we stop our simulation after 2173 turns. Bunches still showing betatron oscillation amplitudes above the 1% acceptance value after 2173 turns are indicated in Figure 8.3 with the value 2173. This is the case for at least one half of the batch. As the blow up was not taken into account for the acceptance check, Figure 8.3 shows a too optimistic estimate in absence of feedback.

The results obtained for the assembled kicker data are worse. However, this is only the case without feedback, as we will see in the next section.

8.3 Use of feedback

For the case with feedback, we will first have a look at the total $1/e$ damping times and the initial betatron oscillation amplitudes, as shown in Figure 8.4. In the most unfavourable case we obtain a total damping time of about $\tau = 1000$ turns. The condition (3.8) is fulfilled, even for the maximum initial betatron oscillation amplitude of $6.31\,\sigma$, because we have a decoherence time of ten times larger than the total damping time. It follows that we can trust the emittances,

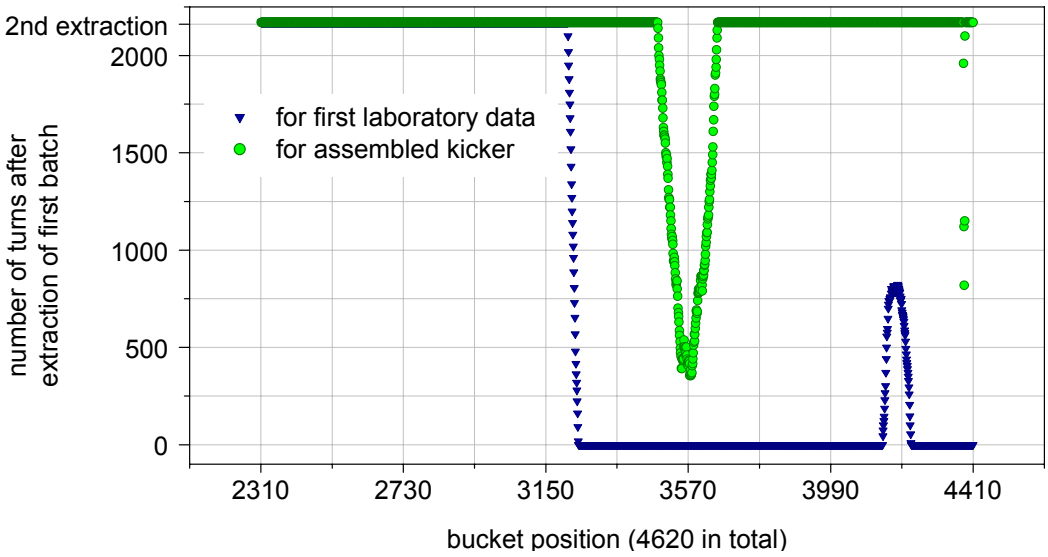

Figure 8.3: Number of turns after extracting the first batch, necessary to meet the CNGS constraints without feedback.

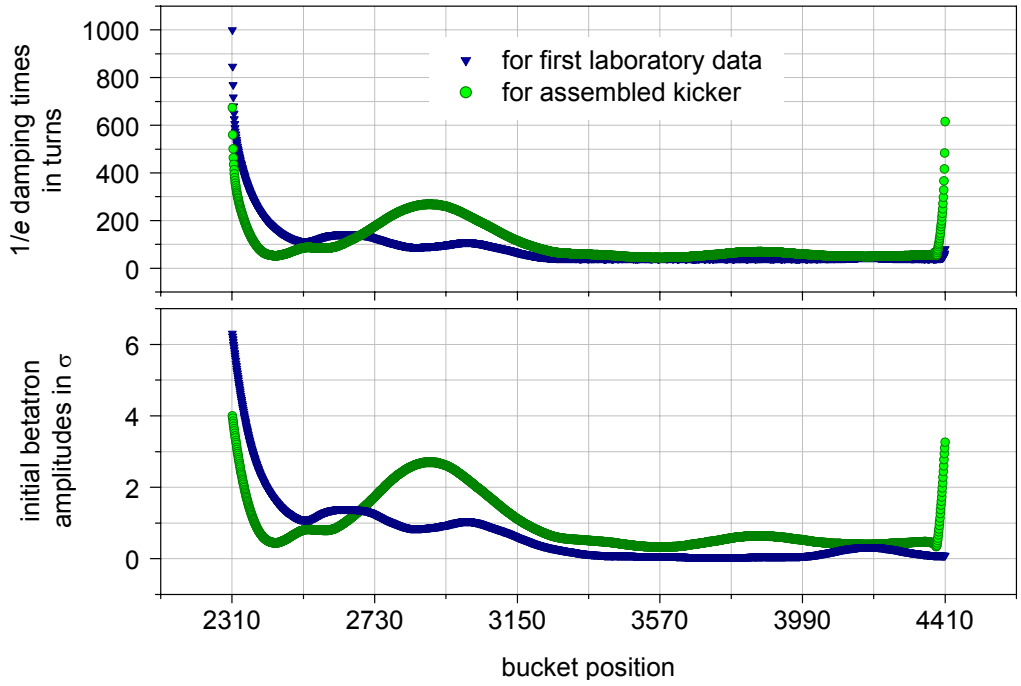

Figure 8.4: The 1/e damping times with feedback and the initial betatron oscillation amplitudes in units of the beam sizes.

determined by the simulation.

The CNGS design value for the normalized emittance is $12\,\mu$m [17]. For the simulation, we assume that the beam emittance has this value at the extraction of the first CNGS batch. Figure 8.5 shows the emittances at the time of the second extraction. In the case where there are no betatron oscillations, the 1 % CNGS target constraint (6.1) corresponds to a maximum acceptable beam emittance of $20.58\,\mu$m. Consequently, the first 2 bunches show a too large emittance at the second extraction, for the first laboratory data of the kicker signal shape. This is not the case for the assembled kicker data.

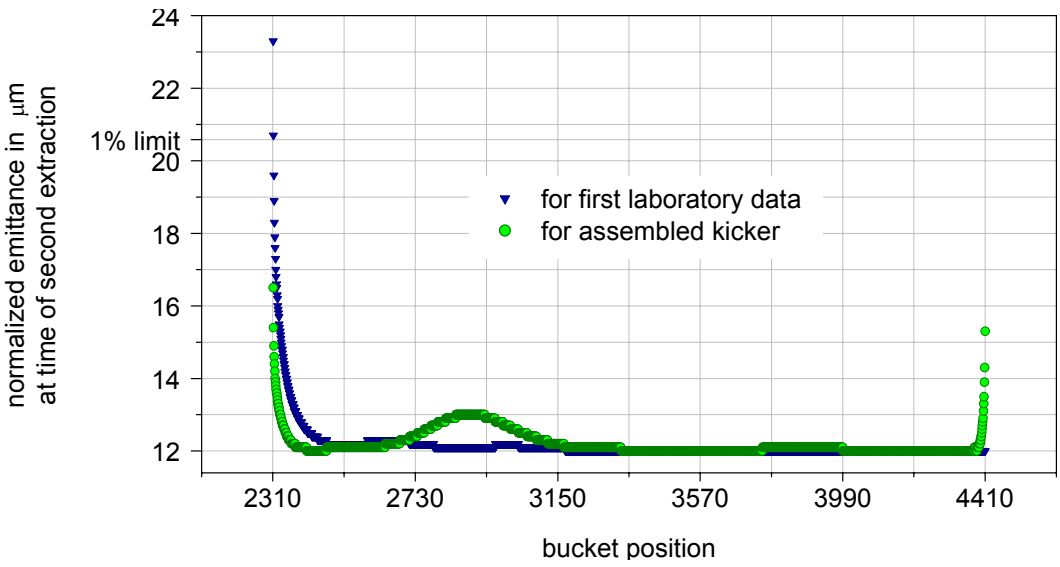

Figure 8.5: Normalized emittances at the time of the second CNGS extraction.

In order to decide whether the CNGS target constraints are fulfilled, we add the normalized beam size increase after the first extraction, and the actual normalized betatron amplitude. The sum of these has to be below the acceptance value ($1.073\sqrt{\mathrm{m}}$) in order to meet the constraint. Results are shown in Figure 8.6. Note that the first two bunches do not fulfill the CNGS con-

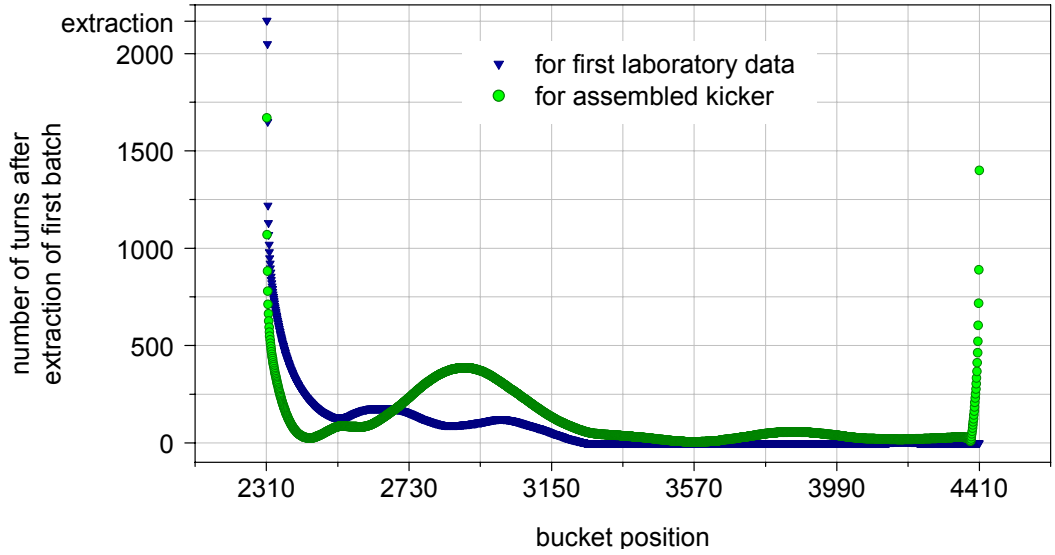

Figure 8.6: Number of turns that the CNGS target constraints are fulfilled with feedback.

straint in the case where we use the first laboratory kicker shape. In the case of the assembled kicker shape, we are able to damp the betatron oscillations quickly enough that after 1670 turns the first bunch will already meet the constraint. This gives a margin of about 30 % in damping time.

The longest times for damping the betatron oscillations are always required for the first and last bunch of the batch. This is due to the bandwidth limitation of the feedback kicker. It results in about 50 % less kick voltage applied to the bunches at the edges, as compared to bunches in the middle of the batch. Therefore, we gain by shorter extraction kicker edges which influence

less the bunches at the edges, even if they give rise to some additional kicks on bunches in the middle of the batch.

8.4 Enlarged gaps between the batches

Increasing the gaps between batches improves the situation very much. In the example, we reduce[1] the number of bunches per batch from 2100 to 2070. This brings a reduction of beam intensity at the CNGS target of 1.4%. At the same time we shorten the extraction kicker length, so that the first and last bunch of the first batch still obtain 99% of the total kick strength. Consequently, the rising edge no longer affects the second batch and the falling edge kicks the first bunch of the second batch with only 5.1% (Figure 8.7). The center of the batch will still

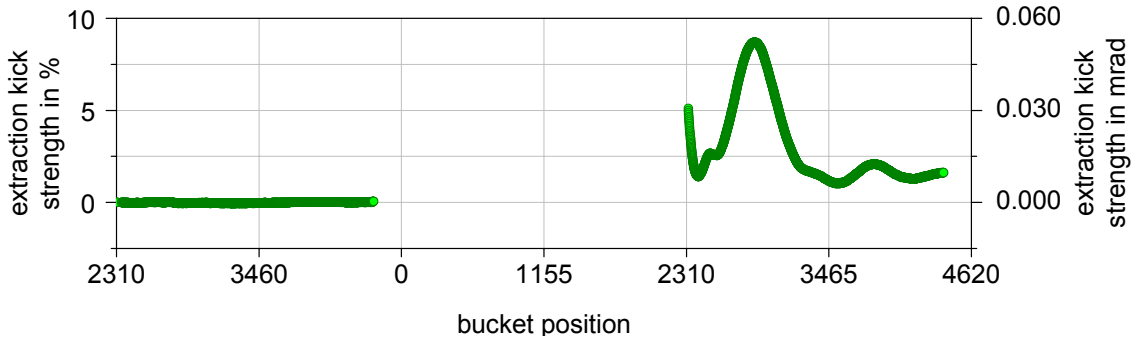

Figure 8.7: Residual kicks on the second batch, caused by the extraction of the first batch, in case of reduction of the number of bunches per batch from 2100 bunches to 2070.

be kicked up to 9 %. Under these circumstances, the second batch already meets the CNGS constraints after 460 turns, which is only a fraction (21 %) of the time between both extractions and gives a comfortable safety margin of 370 % in damping time (Figure 8.8).

8.5 Beam loss

As already pointed out, a bunch oscillating with an amplitude of more that six times the beam size (Figure 8.4) will lose particles at an aperture of eight times the beam size. Using an interpolation function, based on Table 7.1, we calculate from the initial betatron oscillation amplitudes the loss factors for all bunches in the second batch (Figure 8.9).

The calculated losses are very small and it may be difficult in reality to measure them. The total relative intensity loss is $1.6 \cdot 10^{-4}$ per second batch (2100 bunches) using first laboratory data of the extraction kicker signal shape. For the assembled kicker signal shape we find total losses of $1.1 \cdot 10^{-7}$ per second batch (2100 bunches) and $8 \cdot 10^{-9}$ per second batch (2070 bunches).

[1] This does not imply that this filling scheme is operationally possible.

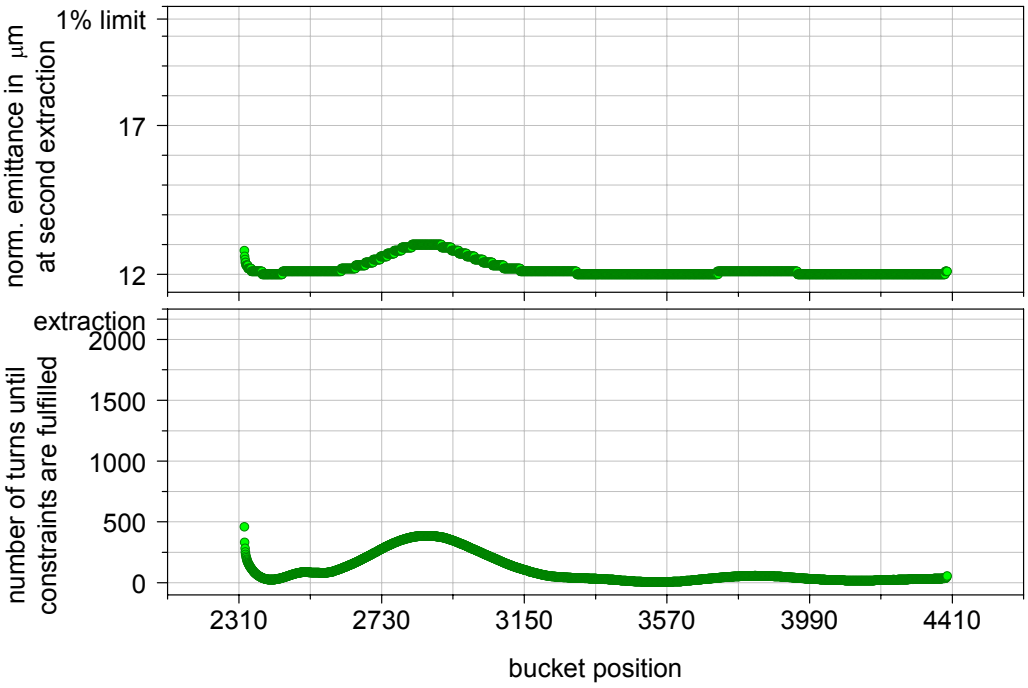

Figure 8.8: Normalized emittance at second extraction and number of turns, required to fulfill the CNGS constraints, when the number of bunches per batch is reduced from 2100 bunches to 2070.

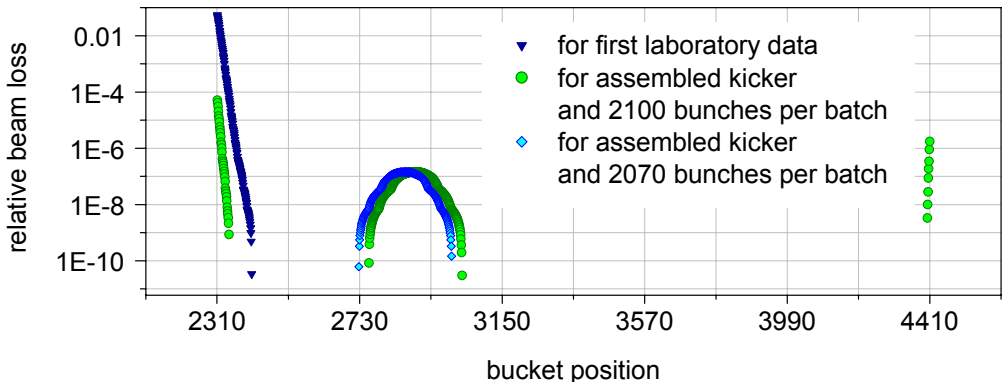

Figure 8.9: Relative beam loss, estimated from the initial betatron oscillation amplitudes after the extraction of the first batch.

Conclusion and Outlook

The first topic of this work was the development of a simulation model, describing the transverse beam-feedback interaction, including the essential technical details of the SPS feedback. This model was then used to analyze whether the SPS feedback system is able to damp the beam oscillations caused by residual kicks on the second CNGS batch during the extraction of the first batch, sufficiently fast to fulfill CNGS constraints (beam on target).

Due to the bandwidth limitation of the final stage amplifier and the high frequency extraction kicker ripples, the damping time varies greatly along the batch.

For ideal CNGS batches in the SPS, i.e. zero population in the two kicker gaps and equal initial intensities and emittances, the effect of the actual residual extraction kick can be cured by the SPS feedback system. As the safety margin is only 30% in time, this has to be verified by machine studies.

Beam losses seem to be negligible in the ideal case. This situation may significantly change in the case of population of the kicker gaps. Particles in the gaps can be kicked directly into the extraction septum. It is proposed that this will be examined during machine studies in 2004.

Machine studies with measurements of the decoherence time, the bunch-by-bunch beam intensity, transverse emittances and betraton oscillation amplitudes turn-by-turn and bunch-by-bunch, can qualify and benchmark the simulation results.

Bibliography

[1] W. Höfle, 'Towards a Transverse Feedback System and Damper for the SPS in the LHC Era', Part. Accel. 58 (1997), pp.269-279 (CERN Report No. CERN-SL-97-017-RF, 1997)

[2] K. Elsener (Editor), M. Buhler-Broglin, K. Elsener, L.A. Lopez Hernandez, G.R. Stevenson, M. Wilhelmsson (Authors), D. Lajust, H.H. Vincke (Preparation), J.-L. Caron (Illustrations), 'General description of the CERN project for a neutrino beam to Gran Sasso (CNGS)', CERN AC Note (2000-03), (December 2000); http://proj-cngs.web.cern.ch/proj-cngs/Download/CNGSDGVE/cngsdgve.pdf

[3] personal communication with G. Arduini, CERN (January 2004)

[4] A. Angermann, M. Beuschel, M. Rau, U. Wohlfarth, Matlab - Simulink - Stateflow, 2. überarbeitete Auflage (Oldenbourg Verlag München Wien, ISBN 3-486-27377-9, 2003)

[5] L. Vos, 'Transverse Emittance Blow-Up from Dipole Errors in Proton Machines', in *Proceedings of the European Particle Accelerator Conference, Stockholm, Sweden,* 1998 (CERN Report No. LHC-Project-Report-193, 1998)

[6] personal communication with L. Vos, CERN (autumn 2003)

[7] K. Wille, Physik der Teilchenbeschleuniger und Synchrotronstrahlungsquellen, (B.G. Teubner Stuttgrt, ISBN 3-519-03087-X, 1992)

[8] W. Höfle, 'Towards a Transverse Feedback System and Damper for the SPS in the LHC Era', presented at the *Workshop on High Brightness Beam for Large Hadron Colliders* in Montreux 1996, Switzerland, Particle Accelerators Vol. 58, 269-279, 1997 (CERN Report No. CERN SL/97-17 (RF), April 1997)

[9] personal communication with E. Gaxiola, CERN (2004)

[10] H. Lutz, W. Wendt, Taschenbuch der Regelungstechnik, (4., korrigierte Auflage, Verlag Harri Deutsch, Frankfurt am Main, ISBN 3-8171-1668-3, 2002)

[11] W. S. Levine (Editor), The Control Handbook, (CRC and IEEE Press, ISBN 0-8493-8570-9, 1996)

[12] K.-D. Kammeyer, K. Kroschel, Digitale Signalverarbeitung - Filterung und Spektralanalyse mit MATLAB-Übungen, (5., durchgesehene und ergänzte Auflage, B.G. Teubner Stuttgrt / Leipzig / Wiesbaden, ISBN 3-519-46122-6, 2002)

[13] R. Bossart, L. Burnod, J. Gareyte, B. de Raad, V. Rossi, 'The Damper for the Transverse Instabilities of the SPS', IEEE Transactions on Nuclear Science, Vol. NS-26, No. 3 (June 1979)

[14] M. Meddahi, at *Twenty-first APC Meeting*, CERN (30. January 2004)

[15] B. Goddard, P. Knaus, G. Schröder, W. Weterings, J. Uythoven, 'The New SPS Extraction Channel for LHC and CNGS', in *Proceedings of the Seventh European Particle Accelerator Conference* (*EPAC 2000*), *Vienna*, 26-30 June 2000 (CERN Report No. CERN-SL-2000-036 BT, 2000)

[16] personal communication with H. Burkhardt, CERN (2004)

[17] CNGS project home page *CERN Neutrinos to Gran Sasso*, CERN (2004), http://proj-cngs.web.cern.ch/proj-cngs/

Acknowledgments

We would like to thank Enrique Gaxiola who initiated the present work by asking us whether the SPS transverse damper is able to cure the betatron oscillations caused by extraction kicker ripple. He also supplied us with measured data of the extraction kicker field.

For fruitful theoretical suggestions we are grateful to Lucien Voss and Helmut Burkhardt. Lucien Voss proposed that an extension of his beam decoherence treatment should be well justified for the case of a transverse feedback in operation. Coffee break conversation with Helmut Burkhardt on collimation problems in the SPS to LHC transfer line gave rise to the idea how to calculate the beam loss in our case.

We would also like to thank Gianluigi Arduini for his interest in the work and providing us with beam data and characteristics such as the order of magnitude of the transverse beam decoherence time.

We also offer our thanks to Patricia Shinnie and Trevor Linnecar for proof-reading, discussions and suggestions.